Gene-specific mechanisms direct Glucocorticoid Receptor-driven repression of inflammatory response genes in macrophages

Maria A. Sacta[1,2,3], Bowranigan Tharmalingam[2], Maddalena Coppo[2], David A. Rollins[2,3], Dinesh K. Deochand[2], Bradley Benjamin[2], Li Yu[4], Bin Zhang[5], Xiaoyu Hu[2,5], Rong Li[6], Yurii Chinenov[2] and Inez Rogatsky[2,3,*]

[1]Weill Cornell/ Rockefeller/ Sloan Kettering Tri-Institutional MD-PhD Program, 1300 York Avenue, New York, NY 10021 USA

[2]Hospital for Special Surgery Research Institute, The David Rosensweig Genomics Center, 535 East 70th Street, New York, NY 10021 USA

[3]Graduate Program in Immunology and Microbial Pathogenesis, Weill Cornell Graduate School of Medical Sciences, 1300 York Avenue, New York, NY 10021 USA

[4]Tsinghua-Peking Center for Life Sciences, Tsinghua University, Beijing 100084 China

[5]Institute for Immunology and School of Medicine, Tsinghua University, Beijing 100084 China

[6]Department of Molecular Medicine, The University of Texas Health Science Center at San Antonio, San Antonio, Texas 78229 USA

***Corresponding author:**

rogatskyi@hss.edu

Tel: 1 212-606-1462

Fax: 1 917-260-4496

Running title: Repression of inflammatory genes by GR

Abstract

The Glucocorticoid Receptor (GR) potently represses macrophage-elicited inflammation, however, the underlying mechanisms remain obscure. Our genome-wide analysis in mouse macrophages reveals that pro-inflammatory paused genes, activated via global negative elongation factor (NELF) dissociation and RNA Polymerase (Pol)2 release from early elongation arrest, and non-paused genes, induced by de novo Pol2 recruitment, are equally susceptible to acute glucocorticoid repression. Moreover, in both cases the dominant mechanism involves rapid GR tethering to p65 at NF-kB binding sites. Yet, specifically at paused genes, GR activation triggers widespread promoter accumulation of NELF, with myeloid cell-specific NELF deletion conferring glucocorticoid resistance. Conversely, at non-paused genes, GR attenuates the recruitment of p300 and histone acetylation, leading to a failure to assemble BRD4 and Mediator at promoters and enhancers, ultimately blocking Pol2 initiation. Thus, GR displays no preference for a specific pro-inflammatory gene class, however, it effects repression by targeting distinct temporal events and components of transcriptional machinery.

Keywords: inflammation; macrophages; glucocorticoid receptor; transcriptional repression; transcription initiation and elongation; RNA Polymerase 2

Introduction

Inflammation is an innate immune response to tissue injury or infection. It relies on macrophages, which recognize pathogen-associated molecular patterns and other 'danger' signals via their toll-like receptors (TLRs) (Glass and Saijo 2010). This initiates a signaling cascade that leads to the activation and DNA binding of the effector transcription factors NF-kB and AP1 (O'Neill et al. 2013) which recruit coregulators, and, ultimately, the basal transcription machinery that together alter the chromatin state in the vicinity of many pro-inflammatory genes and enable their transcription (Smale and Natoli 2014; Glass and Natoli 2015). Acute transcriptional activation of pro-inflammatory genes is, therefore, critical for overriding the homeostatic set-point and producing a robust immune response that helps to resolve infection or tissue injury (Kotas and Medzhitov 2015).

Although the magnitude and dynamics of inflammation is affected at multiple levels, the temporal coordination of cytokine gene transcription by RNA Polymerase (Pol) 2 is a key mechanism that defines acute inflammatory response. The Pol 2 transcription cycle has been divided into three phases: initiation, elongation and termination. Initiation involves the recruitment of Pol 2 to the promoter, histone modifications and changes in histone occupancy. In addition, the C-terminal domain (CTD) of Pol 2, which contains multiple heptad repeats (YS2PTS5PS), is phosphorylated at S5, and Pol 2 synthesizes short (20-60 nt) RNA transcripts. During the elongation step, Pol 2 is further phosphorylated at S2 by the cyclin T1/CDK9 positive transcription elongation factor (P-TEFb) and synthesizes the full length RNA transcript, which is followed by the termination step and RNA transcript dissociation from the DNA (Nechaev and Adelman 2011).

Although Pol 2 recruitment and initiation has been historically considered the rate-limiting step in signal-dependent transcription, numerous recent studies revealed that transcriptionally engaged Pol 2 often remains paused near promoters in the absence of activating signal, and

that entry into productive elongation is rate-limiting for activation of up to 40% of inducible genes (Core et al. 2012). The paused Pol 2 is in a complex with the 4-subunit negative elongation factor (NELF); NELF phosphorylation by P-TEFb leads to its release and Pol 2 entry into productive elongation (Chiba et al. 2010; Nechaev and Adelman 2011). A subset of cytokine genes in macrophages is controlled at the level of Pol 2 pausing. Indeed, while for genes such as Il1a and Il1b, signal-dependent Pol 2 recruitment to their transcription start sites (TSS) and transcription initiation are rate-limiting, other genes, exemplified by Tnf, are occupied by Pol 2 even under resting conditions (Adelman et al. 2009; Hargreaves et al. 2009; Gupte et al. 2013). At Tnf, Pol 2 is S5-phosphorylated, bound by NELF and paused ~50 bp downstream of the TSS. Pause release following S2 and NELF phosphorylation by P-TEFb occurs in response to inflammatory signal.

Aside from Pol 2 occupancy, the chromatin state plays an integral part in the regulation of transcription (Smale et al. 2014). In particular, histone code “writers” such as acetyltransferases (HATs) GCN5 and p300 have been implicated in modifying H3K9/14 and H4K5/8/12 at inflammatory genes in macrophages following treatment with TLR4 ligands (Hargreaves et al. 2009; Escoubet-Lozach et al. 2011). Both HATs are recruited by the NF-kB subunit p65 to regulatory regions in a stimulus-dependent manner (Hargreaves et al. 2009; Ghisletti et al. 2010). Histone modifications are then bound by “readers” such as BRD4, a protein containing two conserved N-terminal bromodomains (BD1 and BD2), which associates with most active promoters and some active enhancers, and has been proposed to couple the acetylation state at enhancers and promoters with Pol 2 elongation (Loven et al. 2013; Brown et al. 2014). BRD4 occupancy correlates with acetylation marks at H4K5/8/12, H3K9/27 (Loven et al. 2013; Kanno et al. 2014; Nagarajan et al. 2014) and with gene activation, whereas chemical inhibition of BRD4 binding abrogates the induction of a subset of genes (Nicodeme et al. 2010). Furthermore, BRD4 has been shown to associate with P-TEFb, affecting Pol 2 CTD phosphorylation, and hence, transcription elongation (Itzen et al. 2014).

These events coalesce ensuring a rapid remodeling of the inflammatory transcriptome, with hundreds of genes undergoing a dramatic upregulation (Escoubet-Lozach et al. 2011; Chinenov et al. 2012; Gupte et al. 2013; Uhlenhaut et al. 2013; Tong et al. 2016). Although essential for host defense, unabated inflammation imposes a threat to the host and can result in tissue damage and autoimmunity. One systemic mechanism that controls acute inflammatory response is a feedback loop whereby inflammatory cytokines trigger the production of steroid hormones known as glucocorticoids (GCs) (reviewed in (Sacta et al. 2016)). Lipophilic GCs diffuse through the cell membrane and bind the intracellular glucocorticoid receptor (GR), a transcription factor (TF), which then translocates to the nucleus and regulates gene expression. The transcriptional outcomes of GR activation are context-specific and are determined by the genomic GC response elements (GRE) to which the receptor binds. GR can bind directly to specific, usually pseudopalindromic, DNA sequences either as a homodimer or complexed with other TFs such as AP1 and STAT3 (Biddie et al. 2011; Langlais et al. 2012). In this context, GR recruits various coregulators such as members of the p160 family, HATs, the Mediator complex and ATP-dependent chromatin remodelers (Weikum et al. 2017b), ultimately leading to the activation of numerous genes including the anti-inflammatory genes, such as *Dusp1* and *Tsc22d3* (GILZ). At other sites, known as “tethering” GREs, GR does not directly bind DNA but interacts with other DNA-bound TFs such as pro-inflammatory AP1 and NF-kB and usually represses their activity (reviewed in (Chinenov et al. 2013)) – a property fundamental to the ability of GCs to dramatically attenuate inflammation. In contrast to GR-mediated activation, the mechanisms of transcriptional repression by GR remain poorly understood. Strikingly, however, in a few cases analyzed, genes activated through Pol 2 recruitment and those induced by signal-dependent Pol 2 pause release were both susceptible to GR-mediated repression (Gupte et al. 2013).

Here, we use a combination of cell-based and genome-wide approaches to elucidate the

mechanisms by which GR represses pro-inflammatory genes in primary macrophages challenged acutely with the TLR4 agonist lipopolysaccharide (LPS) and GCs. We present evidence of 'tethering' as a prevalent mechanism of repression among p65/GR co-regulated genes. We further demonstrate a widespread yet gene class-specific role of NELF in glucocorticoid-mediated repression of early elongation. Conversely, at other genes, GR precludes the ordered assembly of HATs, Brd4 and the Mediator complex which ultimately blocks Pol 2 recruitment and transcription initiation.

Results

Genomic binding of GR and p65 upon inflammatory and anti-inflammatory stimulation

To understand the mechanisms by which GR elicits its repressive effects, we first assessed by RNA-seq the global transcriptional changes upon acute activation of primary mouse bone marrow-derived macrophages (BMDM) with LPS or LPS together with a synthetic GC dexamethasone (Dex) for 1 h. At FDR<0.1 we found that, compared to vehicle-treated BMDM, 597 genes were induced by LPS >1.5 fold. Of these, the induction of 201 genes was attenuated >1.3 fold by Dex co-treatment (Fig. 1A and Supplementary File 1). As expected, GO analysis of acutely GR-repressed genes revealed predominantly those involved in cytokine signaling (Fig. 1A).

Despite rapid remodeling of the macrophage LPS-induced transcriptome in response to Dex observed by us and others (Fig. 1, (Rao et al. 2011; Chinenov et al. 2012; Uhlenhaut et al. 2013; Chinenov et al. 2014)), no comprehensive analysis of the GR and p65 genome-wide occupancy under acutely repressing conditions has been reported. Therefore, we determined the distribution of p65 and GR genomic binding sites in BMDM pulsed with LPS, Dex or LPS+Dex for 45 min (See Fig. 1 - Figure Supplement 1-2 and Supplementary File 2 for quality metrics and comparison of replicates). Following LPS+Dex exposure, we detected 9987 GR peaks (union of two replicates) 5397 (54.1%) of which did not overlap with p65 peaks at the

same conditions (Fig. 1B, top, Fig. 1 - Figure Supplement 1A). Motif overrepresentation analysis in these GR unique peaks revealed predominance of centrally-enriched NR3C binding motifs, which represent GREs and highly related NR binding sites, those for ETS family members, such as the macrophage lineage-determining TF SPI1 (PU.1 and SPIB), and AP1 family members (Fig. 1B, Fig. 1 - Figure Supplement 1B, left panel). The analysis of p65 binding after LPS+Dex treatment revealed 7052 peaks (union of two replicates) of which 2344 (33.8%) were uniquely bound by p65 (Fig. 1B, Fig. 1 - Figure Supplement 2A). Motif analysis indicated an enrichment of NF-kB/Rela binding motifs, as well as ETS and AP1 motifs (Fig. 1B). Importantly, the GR and p65 cistromes shared 4589 peaks, which corresponds to nearly half of all GR- and 2/3 of all p65-binding peaks. Motif analysis of these peaks showed a predominance for NR3C/GRE, ETS family, NF-kB/Rela and AP1 binding motifs that were enriched near the peak summits (Fig. 1B, bottom, Fig. 1 - Figure Supplement 1B, middle panel).

Because of the significant enrichment of peaks with NF-kB elements (especially among those overlapping p65-binding peaks) in the GR cistrome under repressing conditions, we performed GR ChIP-seq in BMDM treated with Dex only for 45 min to compare the two GR cistromes. In Dex-treated BMDM, GR binding sites formed 3377 peaks. Of those, 3165 also appeared in the GR LPS+Dex cistrome (with only 212 peaks unique to Dex-treated BMDM) whereas 6817 were gained in the GR LPS+Dex cistrome (Fig. 1 - Figure Supplement 1A, right panel). ETS and NR3C binding motifs were over-represented in both Dex-unique and Dex – LPS+Dex-shared subsets of GR peaks and trended towards the peak summit (Fig. 1C, Fig. 1 - Figure Supplement 1B, right panel). We did not detect NF-kB/Rela motif enrichment in these two subsets of GR binding peaks. However, among 6817 peaks unique to the GR LPS+Dex cistrome we readily observed an overrepresentation of NF-kB and AP1 motifs while NR3C motifs were no longer enriched (Fig. 1C, compare top/middle vs. bottom motif enrichment panels) indicating that inflammatory signaling and p65/NF-kB activation was driving GR recruitment to such sites specifically under repressing LPS+Dex conditions.

The majority of GR and p65 binding sites were located in distal intergenic (~39-47% of peaks) and intronic (~40% on average) regions (Fig. 1D), similar to previously reported GR and p65 cistromes in various cell lines (Reddy et al. 2009; Barish et al. 2010).

To correlate GR binding with transcriptional outcomes, we focused on our subset of 201 LPS-induced Dex-repressed genes as determined by RNA-seq (Fig. 1A, Supplementary File 1) and evaluated GR peak localization within these genes and 100 Kb of their 5'- and 3'-flanking regions in Dex- and LPS+Dex-treated BMDM. In this subset a somewhat larger fraction (~52%, compared to 39-47% genome-wide) of GR-binding peaks were located in distal intergenic regions, whereas the fraction of peaks in the introns dropped from 40 to 24% compared to whole-genome GR cistrome (Fig. 1D). This shift was not due to a preponderance of shorter introns or genes in Dex-repressed subset (Fig. 1 - Figure Supplement 1C).

Comparison of GR binding near the 201 Dex-repressed genes with an entire GR cistrome shows that a greater fraction of binding sites was unique to the LPS+Dex condition (81% vs. 68%, Fig. 1E) consistent with a disproportional increase in unique binding site utilization among this functionally constrained set of genes. Several representative examples of GR and p65 co-binding near GR-sensitive genes are shown in Fig. 1F: at each gene, GR binding occurred at sites matching those of p65, but only in LPS+Dex and not LPS- or Dex-alone treated BMDM. Importantly, LPS-dependent p65 binding fully persisted in the presence of Dex. In fact, the total number of p65 binding peaks in the presence of LPS and LPS+Dex was comparable both genome-wide, and in the vicinity of our GR-repressed genes (Fig. 1 - Figure Supplement 2A, right and 2B). In each case, ~2/3 of the LPS-induced p65 peaks persisted in LPS+Dex-treated BMDM. Moreover, among p65 LPS+Dex peaks functionally constrained to Dex-repressed genes, 80% (up from 68% genome-wide) overlapped LPS-induced peaks (Fig. 1 - Figure Supplement 2C). Interestingly, of the 201 genes repressed by Dex in the context of LPS-mediated macrophage activation, only 56 were repressed ≥1.3 fold (and only 16 of those ≥2-fold) upon treatment with Dex alone (Supplementary File 1; RNA-seq dataset from (Chinenov et

al. 2014)) – further supporting a requirement for NF-kB activation for GR recruitment to the majority of genes Dex-sensitive genes. Combined, these results further corroborate a tethering model in which p65 is a central component of repression complexes in GC-treated BMDM.

NELF mediates repressive effects of GR at paused genes

We have reported that at several pro-inflammatory genes in unstimulated BMDM, promoter-proximally paused Pol 2 is in a complex with NELF and enters productive elongation following LPS treatment (Adelman et al. 2009; Gupte et al. 2013). To assess how common this type of Pol 2 dynamics is among inflammatory genes, we performed Pol 2 ChIP-seq in untreated, LPS- or LPS+Dex- treated BMDM.

Fig. 2A shows Pol 2 tracks for six genes all of which were among 201 that were rapidly induced by LPS and repressed by Dex as established by RNA-seq (Fig. 1A). Of those, *Tnf*, *Hilpda* and *Btg2*, all display accumulation of Pol 2 near the TSS in untreated BMDM. Upon a 45-min LPS treatment, we detect additional Pol 2 loading and, notably, its redistribution into the body of the gene; conversely, upon LPS+Dex treatment, Pol 2 largely remains near the TSS resembling a 'paused' pattern seen in the unstimulated BMDM (Fig. 2A, left). In contrast, non-paused genes *Il1a*, *Il1b* and *Cd83* display no substantial Pol 2 occupancy in the unstimulated BMDM, and a dramatic and uniform increase in Pol 2 occupancy throughout the gene in response to LPS, which is nearly abrogated by co-treatment with Dex (Fig. 2A, right).

These findings raised the possibility that GR mediates its repressive effects genome-wide by regulating distinct steps of Pol 2 transcription cycle depending on the rate-limiting step for gene activation. To address this possibility, we first calculated Pol 2 pausing indexes (PI) for approximately 300 transcripts corresponding to our 198 LPS-induced Dex-repressed genes (3 genes were excluded due to the conflict of annotation). As described in (Nechaev et al. 2010), we defined PI as the ratio of log-transformed normalized Pol 2 counts around the promoter (-200/+500 bp relative to the annotated TSS) to those within the gene body downstream of +500

bp (Fig. 2B, Supplementary File 3). Based on the PI in untreated BMDM, we classified GC-repressed genes into two groups: 61 transcripts had a PI>1 and were considered to be paused (twice as much of Pol2 at the promoter region versus gene body), whereas 82 had a PI<0.8 and were considered non-paused (see Methods and (Nechaev et al. 2010)). Fig. 2C shows Pol 2 distribution within the -200/+1500 region for individual transcripts of both classes in unstimulated BMDM, as well as BMDM exposed for 45 min to LPS or LPS+Dex. The read density distribution for 61 paused and 82 non-paused transcripts in differentially treated BMDM (Fig. 2D) reveals a peak of Pol 2 occupancy in the promoters of the paused genes, additional Pol 2 loading, and, importantly, its entry into gene bodies in response to LPS. Co-treatment with Dex decreases Pol 2 occupancy in gene body with most Pol 2 remaining near the TSS (Fig. 2C and D). Conversely, little Pol 2 is seen in the non-paused genes in untreated BMDM; Pol 2 occupancy increases dramatically throughout the genes in LPS-treated BMDM and this loading is largely abrogated by Dex (Fig. 2C and D), consistent with the pattern shown in Fig. 2A for representative genes.

Because Pol 2 pausing within the first 100 nt of a gene is mediated by NELF (Adelman and Lis 2012), we assessed genome-wide NELF distribution by ChIP-seq using antibodies to the NELF-E subunit of the complex. Aligned with Pol 2 PI heat maps, NELF-E occupancy matched closely Pol 2 distribution in untreated BMDM with striking accumulation immediately downstream of TSS of paused genes and little to no NELF-E seen in non-paused genes (Fig. 2C and 2D, far right). Indeed, read density distribution in NELF-E ChIP-seq shows highly gene class-specific NELF-E occupancy at paused (PI>1) promoters (Fig. 2D, right).

As reported previously for a few individual genes (Adelman et al. 2009; Schaukowitch et al. 2014), following LPS stimulation, NELF-E was broadly evicted from promoters of LPS-induced genes with little occupancy detected at 1 h (Fig. 3A). Interestingly, however, this dismissal was transient, as despite continued LPS exposure, NELF reloaded onto promoters reaching widespread occupancy by 3 h (Fig. 3A, also see average occupancy graphed for all paused transcripts). This release and reloading can be seen at specific paused GC-sensitive genes,

Tnf, *Hilpda*, and *Btg2* (Fig. 3A, right), which show substantial NELF-E occupancy at the TSS co-localizing with Pol 2 peaks in resting BMDM, its dissociation following a 1-h LPS induction, and re-establishment of the TSS-associated NELF-E peaks by 3 h.

To directly assess whether NELF occupancy in GC-sensitive genes in BMDM correlates with Pol 2 pausing in early elongation, we compared the NELF-E and Pol 2 cistromes in the unstimulated BMDM. Among the LPS-induced Dex-sensitive genes with PI>1 (approximately 24% of 300 Dex-repressed transcripts), 86.3% displayed promoter-associated NELF-E peaks, compared to only 31.7% in genes with PI<0.8 (which comprised approximately 66% of 300 transcripts; Fig. 3B, left). Importantly, similar relative numbers of paused and non-paused genes (23 and 70 %, respectively; Fig. 3 – Figure Supplement 1B) were found among LPS-induced Dex-insensitive genes from RNA-seq (Fig. 1A). In this group, NELF-E occupancy in untreated BMDM was again much more prevalent in paused genes (81.1%) than in non-paused ones (44.2%). Thus, GR does not preferentially repress genes in one class vs. the other, and high levels of TSS-associated NELF in a basal state is a common feature of paused genes irrespective of their sensitivity to GC.

Given that NELF and Pol 2 co-localize at the TSS of the paused genes in unstimulated BMDM, that activation of such genes by LPS coincides with NELF dismissal, and that Pol 2 remains near the promoters of these genes under repressing conditions consistent with their early elongation arrest, we questioned whether GR-mediated repression was globally mediated by NELF. We first evaluated NELF-E occupancy in BMDM co-treated with LPS+Dex by ChIP-seq and found the relative distribution of peaks among paused (PI>1) and non-paused (PI<0.8) repressed genes to be indistinguishable from NELF-E distribution in resting BMDM (83.6% and 33.2%, respectively; Fig. 3B, right – compare to left). We then evaluated NELF-E distribution across several of our target genes in the presence of LPS+Dex and detected striking promoter-proximal NELF peaks in paused *Tnf*, *Myc*, *Errfi1* and *Ccl2*, but not in non-paused *Il1b* or *Lif* (Fig. 3B). To address directly whether NELF is necessary for GR-mediated repression, we used a

new mouse strain conditionally lacking the NELF-B subunit and, hence, the functional NELF complex in myeloid cells (see Methods). BMDM from NELF-B LysM-Cre mice (NELF-B KO) show a dramatic reduction in NELF-B mRNA and protein (Fig. 3C, top). Importantly, as the NELF complex requires all four subunits for stability and the loss of a single subunit leads to the proteolytic degradation of the complex (Gilchrist et al. 2008), immunoblot also reveals a near complete loss of the NELF-E protein in the BMDM of the NELF-B KO (Fig. 3C, top). Using WT and NELF-B KO BMDM, we then compared GR-mediated repression of our candidate GC-sensitive genes. Consistent with the lack of overt phenotype in these mice, RNA-seq of resting BMDM of the two genotypes revealed no significant differences in the expression levels of LPS-induced Dex-repressed genes at baseline (Fig. 3 – Figure Supplement 1C). Moreover, at the time-frame examined, LPS challenge led to a similar induction of *Tnf*, *Myc*, *Errfi1*, *Ccl2*, *Il1b* and *Lif* transcripts irrespective of the genotype (Fig. 3C, bottom left). Interestingly, for all genes classified as 'paused', repression by Dex was significantly attenuated in the NELF-B KO BMDM, but not in non-paused genes *Il1b* and *Lif* (Fig. 3C, bottom right). Collectively, these findings strongly suggest that NELF-mediated block in productive elongation is an integral part of GR-mediated repression of paused genes.

To extend these observations to a whole-genome level, we analyzed transcriptomes from the WT and NELF-B KO BMDM treated with LPS+Dex for 1 h by RNA-seq which identified 393 differentially expressed genes (fold change = 1.5, FDR $p < 0.05$). Out of 201 genes that were repressed by Dex in the WT BMDM (Fig. 1A), 23 were expressed at higher level in the LPS+Dex –treated NELF-B KO BMDM; notably, 21 of them had PI>0.8 (Fig. 3D). Conversely, out of 396 LPS-induced Dex-insensitive genes, only 9 were upregulated in the LPS+Dex-treated NELF-B KO BMDM, 7 of which had PI>0.8 (Fig. 3 – Figure Supplement 1D, left). These observations indicate that NELF ablation disproportionally affects paused LPS-induced Dex-repressed genes.

Because NELF release is triggered by CDK9-mediated phosphorylation, we evaluated the recruitment of CDK9 to the TSS of paused and non-paused genes. Consistent with earlier observations (Luecke 2005), GR inhibited LPS-induced CDK9 recruitment but did so irrespective of the gene class (Fig. 3E) suggesting that NELF retention rather than CDK9 occupancy serves as a defining class-specific feature of glucocorticoid repression of paused genes.

GR-mediated repression of non-paused genes results in attenuation of histone H4 acetylation and BRD4 binding

The dynamics of Pol 2 binding at non-paused genes, as shown in Fig. 2, suggested that the major barrier to activation at these genes is the loading of Pol 2. BMDM surpass this barrier by recruiting NF-kB and AP1 to enhancer regions (Glass and Natoli 2015) that in turn assemble histone modifying proteins, which help create a more permissive chromatin environment for the binding of basal transcriptional machinery and Pol 2. In particular, histone tail modifications, which are associated with both enhancers and promoters are H3K9Ac and H4K5/8/12Ac (Smale et al. 2014). Because these marks correlate with gene transcriptional status, we evaluated the histone acetylation at a subset of our GC-repressed genes of each class.

We noted striking differences in histone tail modifications between representatives of the two gene classes. In particular, paused genes - *Tnf* and *Ccl2* - contained high basal levels of H4PanAc and, specifically, H4K5Ac, at both TSS and kB binding sites which were unaffected by LPS or LPS+Dex treatment (Fig. 4A, bottom row). In contrast, non-paused genes - *Il1b* and *Il1a* - showed a significant increase in H4Ac levels only after LPS treatment, especially at the *Il1b* TSS and two *Il1a* kB enhancers at -10 Kb and -20 Kb, and this increase was fully attenuated by Dex (Fig. 4A, top row).

The change in acetylation seen preferentially at our non-paused genes, appeared to denote a specific “histone code” for histone binding proteins that could potentially affect the

transcription of these genes. In particular, BRD4, the Bromodomain and Extra-Terminal domain (BET) histone binding protein, affects inflammatory cytokine transcription both *in vitro* and *in vivo* through direct binding to acetylated H3 and H4 (Shi and Vakoc 2014). The changes in H4PanAc including H4K5/K12Ac in several GC-sensitive genes, suggested a possible role for BRD4 in transcriptional repression by GR. To test this hypothesis, we first assessed activation of pro-inflammatory genes by LPS in the presence of increasing concentrations of I-BET, an inhibitor of BRD4 binding. The induction of *Il1b* and *Il1a* transcripts was significantly attenuated by I-BET in a dose-dependent manner, whereas *Tnf* and *Ccl2* induction persisted (Fig. 4B). In agreement with gene expression results, ChIP-qPCR experiments revealed that BRD4 was recruited to promoters of non-paused genes *Il1b* and *Il1a* upon LPS treatment and, interestingly, this recruitment was attenuated by Dex (Fig. 4C). Conversely, at the paused genes, *Tnf* and *Ccl2*, BRD4 was readily detectable at the TSS in unstimulated BMDM and this association did not significantly change after either LPS or LPS+Dex treatment. Thus, BRD4 occupancy patterns at the promoters of these genes resembled signal-responsive H4Ac profiles suggesting that loss of BRD4 in response to Dex may underlie GR-mediated repression of, specifically, the non-paused genes.

We then assessed genome-wide distribution of BRD4 by ChIP-seq. Not surprisingly, we observed frequent BRD4 binding across the genome in untreated BMDM (~3700 peaks, Fig 4. – Figure Supplement 1A, left panel). There was a 1.8-fold increase in the number of BRD4 peaks in response to LPS relative to that in untreated BMDM (4345 new peaks, Fig. 4 - Figure Supplement 1A, left panel). The increase in the total peak number was even more apparent when limited to LPS-induced genes: 2.9-fold for Dex-insensitive or -repressed genes (Fig. 4 - Figure Supplement 1A, middle and right panel, respectively). Furthermore, BRD4 loading density specifically at our Dex-sensitive genes increased dramatically in response to LPS which, interestingly, was nearly abrogated by Dex - a trend very apparent at promoters, but also significant at BRD4:p65 shared binding sites (Fig. 4 - Figure Supplement 1B). BRD4 read

366 distribution at individual non-paused genes of interest reflected this dynamics. For example, the
367 *Il1b* TSS and -2.3 Kb and -10 Kb p65 enhancers acquired strong BRD4 binding in response to
368 LPS which was significantly attenuated by Dex, concomitantly with GR loading (Fig. 4D, left top,
369 purple arrows). *Il1a* also displayed increased LPS-induced BRD4 loading at kB-associated
370 upstream enhancers (-10 Kb and -20 Kb) with a dramatic reduction in occupancy upon Dex co-
371 treatment corresponding to GR binding at both regions (Fig. 4D, left bottom, purple arrows).
372 Consistent with our ChIP-PCR data, paused genes, *Ccl2* (-12.5 kB enhancer) and especially *Tnf*
373 (TSS) exhibited modest yet detectable BRD4 occupancy in untreated BMDM that was
374 potentiated by LPS but only minimally affected by Dex (Fig. 4D, right). Moreover, our analysis of
375 BRD4 occupancy at Dex-sensitive genes of the two classes revealed that in paused genes,
376 45% of the BRD4 binding sites seen in LPS-treated BMDM were already pre-bound in untreated
377 cells and 55% were LPS-induced; in non-paused genes, however, only 38% of the sites were
378 pre-occupied in untreated BMDM, whereas 62% were LPS-dependent (Fig. 4E). Thus, our
379 functional studies together with occupancy data suggest that the activation of non-paused
380 genes is more dependent on BRD4 recruitment, and therefore, its dismissal may have a greater
381 impact on genes of this class.

382 Initial BRD4 characterization revealed its interaction with the Mediator complex subunits
383 MED1 and MED12 (Jang et al. 2005; Loven et al. 2013). Mediator is an evolutionarily conserved
384 multi-protein co-activator complex that facilitates transcriptional activation of many genes in part
385 by linking physically and functionally effector TFs and Pol 2. In the context of LPS-induced
386 activation of pro-inflammatory genes, MED1 is reportedly recruited to both the TSS and p65
387 enhancers (Hargreaves et al. 2009; Brown et al. 2014), occupying similar sites across the
388 genome as BRD4, and the two appear to stabilize each other's occupancy at enhancer regions
389 (Loven et al. 2013). We therefore assessed MED1 and MED12 occupancy at the promoters and
390 p65 enhancers of GR-sensitive genes and found that both were recruited to TSS and p65 sites
391 in response to LPS treatment and their recruitment was attenuated by Dex (Fig. 4F). Thus, by

inhibiting BRD4 binding to the TSS and certain enhancer regions at non-paused genes, GR destabilizes MED1 and MED12 occupancy ultimately affecting Pol 2 recruitment. Of note, MED1 and MED12 loss in response to Dex occurred at paused genes as well (Fig. 4F), suggesting that GR may antagonize the Mediator complex binding irrespective of its effects on BRD4.

GR attenuates histone acetylation, cofactor assembly and Pol 2 recruitment to non-paused genes by blocking the recruitment of p300

GR activation disrupted histone acetylation and subsequent BRD4 and Mediator complex assembly at our analyzed non-paused genes, suggesting a central role for LPS-induced histone acetylation as a potential target for GR. Various HATs, including GCN5 and p300, have been implicated in altering modifications at the histone H3 and H4 tails (Smale et al. 2014) Furthermore, p300 has been shown to also interact with and acetylate p65, which contributes to the activation of NF-kB dependent genes (Huang et al. 2009; Nagarajan et al. 2014; Roe et al. 2015). Thus, p300 appeared as a plausible HAT to execute H3/H4 acetylation, thereby dictating the recruitment of BRD4 to the promoters and kB sites of our genes of interest. ChIP-qPCR experiments revealed LPS-dependent recruitment of p300 to the TSS and p65 binding sites of non-paused genes *Il1a* and *Il1b*, which was blocked by Dex. Interestingly, at paused genes, p300 occupancy varied, showing some LPS-potentiated yet Dex-insensitive recruitment to *Tnf*, but a strong constitutive occupancy at *Ccl2* (Fig. 5A). Notably, loss of p300 from these genes did not reflect a simple 'titration' of p300 by the activated GR potentially broadly sequestering it away from kB enhancers, as p300 occupancy at the p65 binding sites of LPS-induced Dex-insensitive genes identified by our RNA-seq analysis - *Cxcl10*, *Cd40*, *Tnfsf9*, *Trim13* - was fully resistant to Dex (Fig. 5B).

We reasoned that p300 catalytic activity rather than its occupancy is a better indicator of whether or not this HAT is involved in regulating target GR-sensitive genes. Therefore, a selective and competitive inhibitor of the p300 HAT activity, C646, was used to determine

418 whether p300-mediated acetylation of histones was necessary for transcriptional activation of
419 candidate pro-inflammatory genes. C646 attenuated in a dose-dependent manner LPS-
420 mediated induction of non-paused genes *Il1b* and *Il1a*, whereas activation of paused genes *Tnf*
421 and *Ccl2* was unaffected (Fig. 5C), consistent with a selective requirement for p300 at the non-
422 paused genes. Furthermore, if GR represses *Il1a* and *Il1b* specifically by precluding p300
423 recruitment, its ectopic introduction into cells should rescue LPS-mediated induction irrespective
424 of GC treatment. Fig. 5D shows that overexpression of wild-type p300 but not its ΔHAT mutant
425 devoid of the catalytic activity in macrophage-like RAW264.7 cells dramatically and specifically
426 reversed GR-mediated repression of non-paused genes. This suggests that GR represses
427 these genes by precluding p300 recruitment, H3/H4 acetylation and the assembly of the BRD4-
428 Mediator complex, ultimately blocking Pol 2 loading.
429
430 **Discussion**
431 Despite the unmatched therapeutic utility of GCs stemming in large part from rapid and direct
432 transcriptional repression of the key inflammatory genes, our knowledge of the overall
433 architecture, dynamics, stability and distribution of such repressive GR complexes in
434 inflammatory cells has been lacking. Given fundamental differences in the rate-limiting events
435 for inflammatory gene activation, we sought to dissect the mechanisms by which GR elicits
436 repression in such distinct gene classes and use genome-wide approaches to assess the
437 generality of our findings.
438 Numerous studies in cell culture and cell-free systems implicated physical interactions
439 between GR, NF-kB and AP1 family members in the inhibition of pro-inflammatory gene
440 transcription (reviewed in (Sacta et al. 2016)) and indeed, we observe extensive co-localization
441 of GR and the NF-kB subunit, p65, genome-wide and especially nearby Dex-repressed genes
442 following short-term LPS+Dex co-treatment – conditions under which we observe rapid
443 glucocorticoid repression. GCs did not cause global displacement of p65; in fact, the number on

p65 binding sites in the presence of LPS vs. LPS+Dex is comparable. Moreover, 80% of p65 peaks associated with our Dex-repressed genes overlap in LPS- and LPS+Dex-treated BMDM. Interaction with p65 is further corroborated by the persistence of p65 peaks near our candidate Dex-repressed genes of both classes. With respect to GR binding, both globally and restricted to Dex-repressed genes, several observations point to a tethering mechanism. First, the predominant motifs enriched in GR peaks present uniquely under LPS+Dex conditions are those of NF-kB and AP1 and not the NR3C motif overrepresented in Dex-treated BMDM or peaks shared between the two cistromes. Second, when compared between an entire genome and restricted to Dex-repressed genes, the fraction of LPS+Dex unique GR binding sites is increasing substantially from 68 to 81%. Third, the majority of the 201 Dex-sensitive genes are only repressed in LPS-activated macrophages, pointing to a requirement for NF-kB activation for GR recruitment. Indeed, the analysis of GR occupancy nearby our candidate Dex-sensitive genes of both classes reveals co-localized GR and p65 peaks associated with NF-kB enhancers under repressing LPS+Dex conditions and no GR binding in Dex-only - treated macrophages. Thus, although this is certainly not the only mechanism by which GR affects inflammatory gene expression (Rao et al. 2011; Uhlenhaut et al. 2013; Oh et al. 2017; Weikum et al. 2017a), tethering to p65 is a widespread regulatory mechanism that GR relies upon to elicit acute repression of pro-inflammatory genes in macrophages.

How GR enacts repression appears to depend on the state of the target promoters prior to activation. At paused genes, Pol 2 is pre-loaded, bound by NELF and “stalled” nearby the TSS, (Gilchrist et al. 2012). These genes have elevated levels of histone acetylation at the TSS, suggestive of an open chromatin state, which would favor constitutive Pol 2 loading and transcription initiation. Conversely, non-paused genes show little Pol 2 occupancy in unstimulated BMDM. Among our Dex-repressed genes, both classes were well represented: in a set of transcripts filtered for Pol 2 occupancy and used to calculate PI, 61 were paused and 82 were not; in a total pool of transcripts corresponding to LPS-induced Dex-repressed 198 genes,

approximately 24% were paused (PI>1) and 66% non-paused (PI<0.8). This distribution matched closely that of genes that were LPS-induced but insensitive to Dex (23% and 70%, respectively), suggesting that GR does not display a preference for a specific gene type for repression.

Given a critical role of NELF in establishing Pol 2 pausing (Gilchrist et al. 2008; Core et al. 2012), we evaluated the genomic distribution of NELF at our LPS-induced Dex-repressed genes in basal, activated and repressed state. This analysis revealed a striking correlation between Pol 2 promoter-proximal pausing and NELF occupancy. Indeed 81% of the paused genes had TSS-associated NELF peaks compared to only 44% on non-paused genes. As expected, NELF dissociated from Pol 2 after LPS treatment, presumably due to P-TEFb-mediated phosphorylation, enabling productive elongation. Although the rate of NELF dismissal varies depending on culture conditions and in our experience takes 30-60 min, this loss is consistently transient as NELF “re-loads” onto the TSS of these genes despite continuous presence of LPS. We previously reported a highly dynamic occupancy of NELF at the *Tnf* promoter (Adelman et al. 2009), but a global synchronous reloading of NELF onto promoters of activated pro-inflammatory genes was unexpected. We envision that NELF re-loading may provide a tonic control of the inflammatory response by limiting further entry of Pol 2 into productive elongation (Aida et al. 2006), yet maintain genes poised for induction by preserving a nucleosome-depleted environment (Gilchrist et al. 2008; Core et al. 2012). A distinct mechanism of ‘tonic control’ of inflammatory gene expression was recently described for a transcriptional repressor Hes1 which limits the recruitment of P-TEFb and hence, NELF release and Pol 2 elongation (Shang et al. 2016). In that regard, it would be informative to examine the dynamics of P-TEFb and phosphorylation of the Pol 2 CTD at the promoters of these genes over the time frame of NELF recycling. Interestingly, paused genes were originally proposed to be fast and transient responders to inducing signals (Adelman et al. 2009; Rogatsky and Adelman 2014); NELF reloading despite prolonged LPS exposure could potentially contribute to cessation of activation

and establishing a ‘tolerant’ LPS-unresponsive state. More generally, our finding illustrates that the transcriptional landscape of macrophages during a sustained exposure to a signal, even in a course of a few hours, undergoes a significant remodeling and a secondary stimulus is likely to elicit variable responses depending on the exact timing of stimulation. Furthermore, given intrinsic macrophage plasticity, whereby a 12-h treatment with a relevant signal (e.g., LPS or Dex) is sufficient to ‘polarize’ them to a distinct myeloid cell population – caution needs to be taken in interpreting results of ‘sequential’ treatments, which may document a response of a reprogrammed macrophage to a new signal rather that simple transcriptional antagonism or synergy.

Under conditions of GC repression, we observed a broad failure of paused genes to release NELF concomitantly with inhibition of Pol 2 entry into productive elongation. Moreover, genetic disruption of NELF resulted in GC resistance of genes in this class establishing a causal relationship between NELF accumulation and GR-mediated repression. Interestingly, NELF was previously shown to participate in estrogen receptor (ER) alpha-mediated gene expression. ERa primarily affects Pol 2 post-initiation steps, whereby pausing is alleviated via hormone-induced recruitment of CDK9 to Pol 2 and NELF and their phosphorylation (Kininis et al. 2008). Given that NRs can dynamically affect P-TEFb occupancy and that P-TEFb recruitment to GC-sensitive genes is attenuated after GC treatment in this and earlier studies (Luecke 2005; Gupte et al. 2013), GR may block elongation by preventing P-TEFb recruitment, possibly through direct steric hindrance. Interestingly, in addition to phosphorylation, NELF has recently been shown to undergo ADP-ribosylation which also facilitates its release (Gibson et al. 2016). It would be informative to assess whether, similar to P-TEFb, ADP-ribosyl transferases that modify NELF are susceptible to regulation by GCs. Finally, a physical interaction between ERa and NELF has been documented at promoters of certain estrogen-activated genes, where NELF recruitment limits the response to hormone (Aiyar 2004). Conceivably, NELF could also serve as a non-conventional “co-repressor” recruited by GR to the promoter-proximal regions of

pro-inflammatory genes in a gene-specific manner. Once recruited, NELF may no longer require GR and assume its known function in Pol 2 pausing. Whether GR-mediated repression involves either of these mechanisms remains to be elucidated.

Interestingly, non-paused genes, such as Il1a and Il1b, exhibit low CpG content, stable nucleosome assembly at promoters, low levels of H3K9/14Ac in the basal state and low TBP occupancy (Ramirez-Carrozzi et al. 2009). This suggests that histone acetylation marks are required for chromatin remodeling which may pose a major barrier to the recruitment of Pol 2 at these genes. We show that an increase in H4Ac at promoters and kB sites in response to LPS correlated with Pol 2 recruitment, and GC attenuated these effects, suggesting that GR may repress these genes by acting upon factors that “write” and “read” histone marks. Among many HATs that modify H3 and H4, p300 is recruited by p65 to the TSS and NF-kB sites and has been shown to acetylate histones that are then bound by BRD4 (Huang et al. 2009; Brown et al. 2014; Nagarajan et al. 2014; Roe et al. 2015). Conceivably, GR attenuates p300 loading by competing for a tethering site on p65 as has been previously documented for IRF3 (Ogawa et al. 2005). We cannot exclude the possibility that additional HATs, i.e., GCN5, contribute to writing H3/H4Ac at our GC-sensitive pro-inflammatory genes.

Given its role as a histone binding protein that reportedly contributes to recruiting P-TEFb and couples the acetylation state at promoters and enhancers with Pol 2 elongation, a clear bias for LPS-induced novel sites of BRD4 recruitment and their sensitivity to Dex specifically at non-paused genes was unexpected. BRD4 binding at promoters broadly correlates with gene activation (Nicodeme et al. 2010; Loven et al. 2013; Brown et al. 2014; Kanno et al. 2014). We now show that similar to I-BETs, GR inhibits, albeit indirectly, loading of BRD4 particularly at non-paused genes and, by exploiting their dependency on histone acetylation, disrupts interactions with Mediator, ultimately antagonizing Pol 2 recruitment and transcription initiation. Because this effect is far from uniform, and some p65/BRD4-bound LPS-induced enhancers are more sensitive to the effects of Dex than others, we speculate that a subset of p65 binding sites

548 has greater functional consequences for gene activity. Identifying a subpopulation of “dominant”
549 enhancers whose BRD4 occupancy is a definitive predictor of transcriptional state, and
550 correlating those with sites of GR recruitment would likely sharpen the differences in BRD4
551 behavior between the two gene classes.

552 Finally, although the two classes of genes are activated and repressed through distinct
553 mechanisms, the consequences of GR activation share commonalities including a failure to
554 recruit P-TEFb and the Mediator complex. P-TEFb is required for gene activation post Pol 2
555 loading, so at non-paused genes failing to recruit Pol 2, P-TEFb loss would have little functional
556 consequences. Conversely, a block in Mediator recruitment at both the TSS and kB sites could
557 potentially contribute to repression of both classes of genes. Mediator is a multi-subunit complex
558 that interacts with numerous activators and components of basal transcription machinery
559 including Pol 2 (Malik and Roeder 2010). With respect to non-paused genes, Mediator interacts
560 directly with both BRD4 and p300, with Mediator and BRD4 stabilizing each other’s occupancy
561 (Jang et al. 2005; Malik and Roeder 2010; Shi and Vakoc 2014). Furthermore, Mediator and
562 p300 can act cooperatively to alter the chromatin landscape and facilitate PIC formation (Malik
563 and Roeder 2010). Although the contribution of Mediator to activation of pro-inflammatory
564 paused genes needs further study, it has been suggested that Mediator may help recruit P-
565 TEFb indirectly promoting pause release (Lu et al. 2016). Additionally, because kB sites are
566 typically distant from promoters, and pro-inflammatory genes were proposed to be activated
567 through DNA looping (Tong et al. 2016), Mediator (perhaps together with Brd4) may contribute
568 to bridging promoters with NF-kB enhancers. Thus, it is tempting to speculate that by hindering
569 Mediator assembly, GR globally disrupts promoter-enhancer communication thereby attenuating
570 pro-inflammatory gene expression.

571

572 **Materials and methods**

573 *Cell culture and reagents*

BMDM were prepared from 8-10 wk old mice as in (Gupte et al. 2013). RAW264.7 cells were cultured in DMEM media (Corning, cat# 10-013-CV) supplemented with 10% fetal bovine serum (Atlanta Biologicals cat# S11550). Dex and LPS were purchased from Sigma.

Transgenic mice

C57BL/6 mice (NCI, Charles River Laboratories), C57BL/6 *Lys2-Cre* mice -/-:*Nelfb* fl/fl mice and their derivatives were maintained in the Weill Cornell Animal Facility in compliance with guidelines from the Weill Cornell Animal Care and Use Committee. All studies were performed on 8-12 wk old male mice.

To create the NELF-B conditional KO strain, NELF-B fl/fl mice (with NELF-B exon 4 floxed (Amleh et al. 2009)) were bred to C57BL/6-derived LysM-Cre mice (Jackson Laboratories, 004781) to obtain double heterozygous LysM-Cre/wt:NELF-B fl/wt (LysM-Cre:HET) animals. To create homozygous (LysM-Cre:NELF-B fl/fl) animals, we self-crossed LysM-Cre-Het mice. The genotype of the progeny was determined using PCR primers described in (Amleh et al. 2009). LysM-Cre primers were obtained from Jackson Laboratories.

Inhibitor experiments

BMDM were plated in 6-well plates at $2*10^6$ cells/well. For BRD inhibitor experiments, cells were pretreated with I-BET (Calbiochem, 401010) for 30 min, followed by co-treatment with LPS (10 ng/ml). For p300 inhibitor experiments, cells were treated with LPS for 30 min, followed by co-treatment with C646 (Abcam, ab142163) for 1 h. Concentrations of inhibitors are shown in Figure Legends.

Transfections

RAW264.7 cells were plated at $2*10^5$ cells/well in 24-well plates and transfected ON using Turbofect (Thermo Scientific, R0531) as per manufacturer's instructions. Cells were treated the

following day as described in Figure Legends. Plasmids used are pcDNA3.1-p300, pcDNA3.1-300(HAT-) (Addgene, Plasmid #23252 and #23254, respectively) and pcDNA3.1 to equalize total amount of transfected DNA.

RNA isolation and Real-time qPCR

Total RNA isolation from BMDM (Qiagen RNAeasy Kit), random-primed cDNA synthesis, and qPCR with Maxima Sybr Green/ROX/2x master mix (Fermentas) on StepOne Plus real time PCR system were performed using standard protocols. Data analysis was performed using the ddCT method. All data was normalized to Actb as housekeeping control. Primers are listed in Supplemental File 4.

Immunoblotting

Whole cell extracts were prepared in RIPA buffer (10 mM Tris-HCl pH 8.0, 1 mM EDTA, 0.5 mM EGTA, 140 mM NaCl, 5% glycerol, 0.1% Na deoxycholate, 0.1% SDS, 1% Triton X-100). Immunoblotting was performed with rabbit polyclonal antibodies to NELF-B (Cell Signaling, 1:2000, 1489S), NELF-E (Proteintech, 1:2000, 10705-1-AP), HSP90 (Cell Signaling 1:200, 4874S).

ChIP

BMDM were treated for 45 min as specified in Figure Legends and single cross-linked in 1% methanol-free formaldehyde for 10 min at RT (AcH4) or double cross-linked using 2 mM disuccinimidyl glutarate (Proteochem, c1104) for 30 min followed by 1% methanol-free formaldehyde for 10 min at RT (CDK9, BRD4, MED1, MED12, p300). The reaction was quenched by 0.125 M glycine for 5 min. Cells were then washed with PBS, scraped and lysed for 10 min at 4°C in lysis buffer with protease inhibitor cocktail. The nuclear extracts were collected by centrifugation at 600*g for 10 min. Nuclei were then washed for 10 min at 4°C in

wash buffer with protease inhibitors and collected as described above. Nuclei were lysed in lysis buffer for 10 min and sonicated to fragment chromatin using 15-18 cycles (30 sec 'on', 30 sec 'off') in a Bioruptor at 4°C. For CDK9, nuclei were sonicated with Covaris S220 Ultrasonicator according to manufacturer's instructions (130 µl shearing buffer, 200 cycles/burst, 120 sec, DF 10). Lysates were cleared by centrifugation at 14,000*g, 20 min, 4°C, and then incubated with normal rabbit IgG (Santa Cruz Biotech, sc-2027x), BRD4 (Abcam, ab84776 and Bethyl Laboratories, A3001-985A100), MED12 (Bethyl Laboratories, A300-774A), MED1 (Bethyl Laboratories, A300-793), p300 (Santa Cruz Biotech, sc-585X), Anti-AcH4 (Millipore, 06-866), Anti-AcH4K12 (Millipore, 07-595), Anti-AcH4K5 (Millipore, 07-327) and 40 µl of 50% protein A/G plus agarose (Santa Cruz Biotech, sc-2003) per reaction at 4°C ON. Beads were washed 4x with RIPA buffer and once with TE buffer. For CDK9, 5 µg of antibodies (Santa Cruz Biotech, sc-8338X or sc-13130X) were pre-bound to 40 µl of Dynabeads Protein A (Invitrogen), washed 2x with beads blocking buffer and incubated with lysates at 4°C ON; IPs were washed 6x with modified RIPA buffer containing 100 mM LiCl on a magnetic stand and once with TE buffer+50 mM NaCl. Each reaction was then incubated in TE+0.5% SDS+200 µg/ml proteinase K (Invitrogen, 25530049) for 2 h at 55°C, followed by 6 h at 65°C to reverse crosslinks. DNA was purified using phenol-chloroform extraction and ethanol precipitation or using Qiagen PCR purification kit. Recruitment at binding sites was assessed by qPCR. All data at putative binding sites was normalized to 28S ribosomal RNA as control. Primers are listed in Supplemental File 4.

ChIP-seq

For GR (Santa Cruz Biotech, sc-1004X), BRD4 (Abcam, ab84776) and p65 (Santa Cruz Biotech, sc-372X) ChIP-seq, nuclei were sonicated with Covaris S220 sonicator according to manufacturer's instructions (130 µl shearing buffer, 200 cycles/burst, 120 sec, DF 10). For Pol 2 (Santa Cruz Biotech, sc-9001X) and NELF-E (Proteintech, 10705-1-AP) ChIP-seq, cells were

formaldehyde cross-linked and nuclei were sonicated as above to obtain fragments in 150-500 bp range. Input DNA was prepared from sonicated material saved prior to IP. Lysates were cleared by centrifugation at 14,000 rpm, 20 min, 4°C, and then incubated with respective antibodies using 40 µl of 50% protein A/G PLUS agarose beads (for GR, BRD4 and Pol 2) or 60 µl of Dynabeads (Invitrogen) (for p65) per reaction at 4°C ON. GR, BRD4 and Pol 2 IPs were then processed as described for ChIP-qPCR above. p65 IPs were washed 6x with modified RIPA buffer containing 100 mM LiCl on a magnetic stand and once with TE buffer+50 mM NaCl and processed as described for ChIP-qPCR above. The efficiency of ChIP was assessed by qPCR. The integrity and quality of DNA was evaluated with Bionalyzer 2100 (Agilent Technologies) before using 10 ng of material to prepare Illumina-compatible sequencing libraries using Illumina Truseq ChIP sample prep kit. Library preparation and sequencing was performed by Weill Cornell Epigenomics Core. Libraries were sequenced by a HiSeq 2500 (50 bp, single-end).

RNA-seq

BMDM from LysM-Cre:NELF-B wt/wt (WT) and/or LysM-Cre:NELF-B fl/fl (NELF-B KO) mice were treated as indicated in individual figure legends (vehicle, LPS, LPS+Dex for 1 h) and RNA was isolated using Qiagen RNA-easy kit. Total RNA was polyA enriched and converted into Illumina-compatible sequencing library with TruSeq mRNA-Seq sample preparation kit (Illumina). Quality control of RNA and libraries was performed using the BioAnalyzer 2100. Pair-end sequencing was performed at the Weill Cornell Epigenomics Core using HiSeq2500.

Quantification and Statistical Analysis

General experimental design and statistical analysis

To ensure reproducibility all *in vitro* experiments were repeated at least in triplicates. The differences between continuous variables were assessed using Student's *t* Test and the differences between discrete variable were assessed with Fisher's exact test.

Real time PCR

Two-tailed Student's t-test was used to ascertain the differences between means as detailed in Figure Legends.

ChIP-seq

Sequencing quality control was performed using FASTQC; adapters, when needed, where trimmed using trimmomatic. 50 bp single-end reads were aligned to the mouse genome (mm10) using CLC Bio Genomic Workbench (GR, Pol 2) or bowtie2 (p65, NELF-E, BRD4). Aligned BAM files were converted into bigwig format for data visualization purposes. The quality of Chip-seq experiments was assessed using ChIPQC package (Carroll et al. 2014) (Supplemental File 2). Cross-correlation analysis, Relative Strand Correlation (RSC) and Normalized Strand Cross-correlation coefficient (NSC) for all ChIP-seq datasets used in this study were calculated with CLC BIO genomics workbench (Fig. 1 - Figure Supplement 1D and 2C; Fig. 3 - Figure Supplement 1A and Fig. 4 - Figure Supplement 1C, Supplemental File 2) as described in (Marinov et al. 2013). RSC reflects the ratio of the fragment-size peaks and the read-size peak in cross-correlation plot. For all experiments with the exception of one NELF-E condition, the RSC is larger than 0.8 as per ENCODE recommendations (Landt et al. 2012). Peak calling was performed with CLC Bio Genomics Workbench (Pol 2) or MACS2 (Zhang et al. 2008) (--gsize 2150570000 --bw=300 --ratio 1.0 --slocal 1000 --llocal 10000 --keep-dup 1 --bdg --qvalue 0.05) with a matching input file to estimate background read distribution.

Peak annotation relative to known genomics features was performed using *ChIPpeakAnno package (R, Bioconductor)* (Zhu et al. 2010) with *TxDb.Mmusculus.UCSC.mm10.knownGene* annotation (2016-09-29 04:05:09 +000). Peak overlaps between datasets were determined using *subsetByOverlap* function from GenomicRanges package (R, Bioconductor) with the minimum

overlap of 1 nt and visualized with *makeVennDiagram* function from *ChIPpeakAnno* (Zhu et al. 2010) package.

Ab initio analysis of overrepresented sequences in ChIP-seq peaks was performed using MEME-ChIP suite with MEME (long sequences), DREME (short sequences) and CentriMO (centrally-enriched sequences). E-values estimate the expected number of motifs in an experimental set of sequences compared to random sequences of the similar size. Sequencing motifs with E-values under 0.0001 were considered statistically significant.

Pol 2 pausing indexes (PI) were calculated as previously described (Nechaev et al. 2010). All transcripts for LPS-induced Dex-sensitive genes present in *TxDb.Mmusculus.UCSC.mm10.knownGene* annotation were filtered to collapse all annotated transcripts with identical 5' ends to a single gene model. For remaining transcripts, the PI was calculated as the ratio of log-transformed, length-normalized read counts at the 5' end flanking region (-200:+500) and transcript "body" (+500: end of a transcript). To compare between replicates, the PI were normalized to respective library sizes (as in Fig. 2B). Read distributions in the region of interest ("promoters" and gene "bodies") were visualized in the form of "heat" maps that show scores (coverage) at a given sequence position or bin using *genomation* package (R, Bioconductor) (Akalin et al. 2014). For heat maps visualization, paused and non-paused transcripts were further filtered by selecting only those that had overlapping Pol 2 peaks in the "promoter" area in LPS-treated BMDM. To summarize read distributions, we plotted mean coverages (*plotMeta, genomation*) over regions of interest (Fig. 2D, 3A and Fig. 4 - Figure Supplement 1B) with the standard error and the 95% confidence interval bands.

RNA-seq

RNA-seq analysis has been performed as previously described (Coppo et al. 2016). 50-bp paired reads were mapped to annotated mouse genome (mm10) with CLC Bio Genomic Workbench (Qiagen). Read count table containing unique exon reads was analyzed using EdgeR (Robinson et al. 2009) package to determine differentially expressed genes. Read

counts were scale normalized using the weighted trimmed mean method and expressed as log-transformed counts per million (cpm). All genes with unadjusted p-value <0.01 (p<0.05 for NELF-B KO experiment) and fold change >1.5 in at least one pairwise comparison were considered to be differentially expressed and were selected for further analysis.

Accession numbers

All raw sequence data generated in this study are deposited to NCBI GEO.

ChIP-seq data: GSE109131 https://www.ncbi.nlm.nih.gov/geo/query/acc.cgi?acc=GSE109131
RNA-seq data:

Acknowledgements

We are grateful to C.E. Mason and J.A. Gandara (Weill Cornell) and S. Mimouna (HSS) for technical help. We acknowledge help from the A. Alonso, Y. Li and the staff of Weill Cornell Epigenomics core. We thank S. Mimouna for helpful discussion. M.A.S is supported by the NIH Diversity Supplement 3R01DK099087-01A1S1 and the MSTP grant T32GM007739 from the NIH NIGMS to the Weill Cornell/ Rockefeller/ Sloan-Kettering Tri-Institutional MD-PhD Program. This work is supported by the grants to I.R. from NIH R01DK099087, the Rheumatology Research Foundation Research Grant, the DOD CDMRP PR130049 Research Award and The Hospital for Special Surgery David Rosensweig Genomics Center. X.H is supported by the Ministry of Science and Technology of China National Key Research Project 2015CB943201, National Natural Science Foundation grants 81422019, 81571580, 91642115, 8151101184, and funds from Tsinghua-Peking Center for Life Sciences. R.L. is supported by the NIH R01CA220578.

Competing interests

The authors declare no conflict of interest

References

Adelman K, Kennedy MA, Nechaev S, Gilchrist DA, Muse GW, Chinenov Y, Rogatsky I. 2009. Immediate mediators of the inflammatory response are poised for gene activation through RNA polymerase II stalling. *Proceedings of the National Academy of Sciences of the United States of America* **106**: 18207-18212.

Adelman K, Lis JT. 2012. Promoter-proximal pausing of RNA polymerase II: emerging roles in metazoans. *Nature Reviews Genetics* **13**: 720-731.

Aida M, Chen Y, Nakajima K, Yamaguchi Y, Wada T, Handa H. 2006. Transcriptional pausing caused by NELF plays a dual role in regulating immediate-early expression of the junB gene. *Molecular and cellular biology* **26**: 6094-6104.

Aiyar SE. 2004. Attenuation of estrogen receptor -mediated transcription through estrogen-stimulated recruitment of a negative elongation factor. *Genes & development* **18**: 2134-2146.

Akalin A, Franke V, Vlahovi ek K, Mason CE, Schubeler D. 2014. genomation: a toolkit to summarize, annotate and visualize genomic intervals. *Bioinformatics* **31**: 1127-1129.

Amleh A, Nair SJ, Sun J, Sutherland A, Hasty P, Li R. 2009. Mouse Cofactor of BRCA1 (Cobra1) Is Required for Early Embryogenesis. *PloS one* **4**: e5034.

Barish GD, Yu RT, Karunasiri M, Ocampo CB, Dixon J, Benner C, Dent AL, Tangirala RK, Evans RM. 2010. Bcl-6 and NF- B cistromes mediate opposing regulation of the innate immune response. *Genes & development* **24**: 2760-2765.

Biddie Simon C, John S, Sabo Pete J, Thurman Robert E, Johnson Thomas A, Schiltz RL, Miranda Tina B, Sung M-H, Trump S, Lightman Stafford L et al. 2011. Transcription Factor AP1 Potentiates Chromatin Accessibility and Glucocorticoid Receptor Binding. *Molecular Cell* **43**: 145-155.

Brown JD, Lin CY, Duan Q, Griffin G, Federation AJ, Paranal RM, Bair S, Newton G, Lichtman AH, Kung AL et al. 2014. NF-kappaB directs dynamic super enhancer formation in inflammation and atherogenesis. *Mol Cell* **56**: 219-231.

Carroll TS, Liang Z, Salama R, Stark R, de Santiago I. 2014. Impact of artifact removal on ChIP quality metrics in ChIP-seq and ChIP-exo data. *Frontiers in genetics* **5**: 75.

Chiba K, Yamamoto J, Yamaguchi Y, Handa H. 2010. Promoter-proximal pausing and its release: Molecular mechanisms and physiological functions. *Experimental Cell Research* **316**: 2723-2730.

Chinenov Y, Coppo M, Gupte R, Sacta MA, Rogatsky I. 2014. Glucocorticoid receptor coordinates transcription factor-dominated regulatory network in macrophages. *BMC Genomics* **15**: 656.

Chinenov Y, Gupte R, Dobrovolna J, Flammer JR, Liu B, Michelassi FE, Rogatsky I. 2012. Role of transcriptional coregulator GRIP1 in the anti-inflammatory actions of glucocorticoids. *Proceedings of the National Academy of Sciences of the United States of America* **109**: 11776-11781.

Chinenov Y, Gupte R, Rogatsky I. 2013. Nuclear receptors in inflammation control: Repression by GR and beyond. *Molecular and Cellular Endocrinology* **380**: 55-64.

Coppo M, Chinenov Y, Sacta MA, Rogatsky I. 2016. The transcriptional coregulator GRIP1 controls macrophage polarization and metabolic homeostasis. *Nature Communications* **7**: 12254.

800 Core LJ, Waterfall JJ, Gilchrist DA, Fargo DC, Kwak H, Adelman K, Lis JT. 2012. Defining the
801 status of RNA polymerase at promoters. *Cell reports* **2**: 1025-1035.
802 Escoubet-Lozach L, Benner C, Kaikkonen MU, Lozach J, Heinz S, Spann NJ, Crotti A, Stender
803 J, Ghisletti S, Reichart D et al. 2011. Mechanisms establishing TLR4-responsive
804 activation states of inflammatory response genes. *PLoS Genet* **7**: e1002401.
805 Ghisletti S, Barozzi I, Mietton F, Polletti S, De Santa F, Venturini E, Gregory L, Lonie L, Chew
806 A, Wei CL et al. 2010. Identification and characterization of enhancers controlling
807 the inflammatory gene expression program in macrophages. *Immunity* **32**: 317-328.
808 Gibson BA, Zhang Y, Jiang H, Hussey KM, Shrimp JH, Lin H, Schwede F, Yu Y, Kraus WL.
809 2016. Chemical genetic discovery of PARP targets reveals a role for PARP-1 in
810 transcription elongation. *Science* **353**: 45-50.
811 Gilchrist DA, Fromm G, dos Santos G, Pham LN, McDaniel IE, Burkholder A, Fargo DC,
812 Adelman K. 2012. Regulating the regulators: the pervasive effects of Pol II pausing
813 on stimulus-responsive gene networks. *Genes & development* **26**: 933-944.
814 Gilchrist DA, Nechaev S, Lee C, Ghosh SK, Collins JB, Li L, Gilmour DS, Adelman K. 2008.
815 NELF-mediated stalling of Pol II can enhance gene expression by blocking promoter-
816 proximal nucleosome assembly. *Genes Dev* **22**: 1921-1933.
817 Glass CK, Natoli G. 2015. Molecular control of activation and priming in macrophages.
818 *Nature immunology* **17**: 26-33.
819 Glass CK, Saijo K. 2010. Nuclear receptor transrepression pathways that regulate
820 inflammation in macrophages and T cells. *Nature Reviews Immunology* **10**: 365-376.
821 Gupte R, Muse GW, Chinenov Y, Adelman K, Rogatsky I. 2013. Glucocorticoid receptor
822 represses proinflammatory genes at distinct steps of the transcription cycle.
823 *Proceedings of the National Academy of Sciences* **110**: 14616-14621.
824 Hargreaves DC, Horng T, Medzhitov R. 2009. Control of inducible gene expression by
825 signal-dependent transcriptional elongation. *Cell* **138**: 129-145.
826 Huang B, Yang XD, Zhou MM, Ozato K, Chen LF. 2009. Brd4 coactivates transcriptional
827 activation of NF-kappaB via specific binding to acetylated RelA. *Mol Cell Biol* **29**:
828 1375-1387.
829 Itzen F, Greifenberg AK, Bosken CA, Geyer M. 2014. Brd4 activates P-TEFb for RNA
830 polymerase II CTD phosphorylation. *Nucleic acids research* **42**: 7577-7590.
831 Jang MK, Mochizuki K, Zhou M, Jeong HS, Brady JN, Ozato K. 2005. The bromodomain
832 protein Brd4 is a positive regulatory component of P-TEFb and stimulates RNA
833 polymerase II-dependent transcription. *Mol Cell* **19**: 523-534.
834 Kanno T, Kanno Y, LeRoy G, Campos E, Sun HW, Brooks SR, Vahedi G, Heightman TD, Garcia
835 BA, Reinberg D et al. 2014. BRD4 assists elongation of both coding and enhancer
836 RNAs by interacting with acetylated histones. *Nat Struct Mol Biol* **21**: 1047-1057.
837 Kininis M, Isaacs GD, Core LJ, Hah N, Kraus WL. 2008. Postrecruitment Regulation of RNA
838 Polymerase II Directs Rapid Signaling Responses at the Promoters of Estrogen
839 Target Genes. *Molecular and cellular biology* **29**: 1123-1133.
840 Kotas ME, Medzhitov R. 2015. Homeostasis, inflammation, and disease susceptibility. *Cell*
841 **160**: 816-827.
842 Landt SG, Marinov GK, Kundaje A, Kheradpour P, Pauli F, Batzoglou S, Bernstein BE, Bickel
843 P, Brown JB, Cayting P et al. 2012. ChIP-seq guidelines and practices of the ENCODE
844 and modENCODE consortia. *Genome research* **22**: 1813-1831.

Langlais D, Couture C, Balsalobre A, Drouin J. 2012. The Stat3/GR Interaction Code: Predictive Value of Direct/Indirect DNA Recruitment for Transcription Outcome. *Molecular Cell* **47**: 38-49.

Loven J, Hoke HA, Lin CY, Lau A, Orlando DA, Vakoc CR, Bradner JE, Lee TI, Young RA. 2013. Selective inhibition of tumor oncogenes by disruption of super-enhancers. *Cell* **153**: 320-334.

Lu X, Zhu X, Li Y, Liu M, Yu B, Wang Y, Rao M, Yang H, Zhou K, Wang Y et al. 2016. Multiple P-TEFbs cooperatively regulate the release of promoter-proximally paused RNA polymerase II. *Nucleic acids research* **44**: 6853-6867.

Luecke HF. 2005. The glucocorticoid receptor blocks P-TEFb recruitment by NF B to effect promoter-specific transcriptional repression. *Genes & development* **19**: 1116-1127.

Ma W, Noble WS, Bailey TL. 2014. Motif-based analysis of large nucleotide data sets using MEME-ChIP. *Nature Protocols* **9**: 1428-1450.

Malik S, Roeder RG. 2010. The metazoan Mediator co-activator complex as an integrative hub for transcriptional regulation. *Nature Reviews Genetics* **11**: 761-772.

Marinov GK, Kundaje A, Park PJ, Wold BJ. 2013. Large-Scale Quality Analysis of Published ChIP-seq Data. *G3: Genes|Genomes|Genetics* **4**: 209-223.

Nagarajan S, Hossan T, Alawi M, Najafova Z, Indenbirken D, Bedi U, Taipaleenmaki H, Ben-Batalla I, Scheller M, Loges S et al. 2014. Bromodomain protein BRD4 is required for estrogen receptor-dependent enhancer activation and gene transcription. *Cell reports* **8**: 460-469.

Nechaev S, Adelman K. 2011. Pol II waiting in the starting gates: Regulating the transition from transcription initiation into productive elongation. *Biochim Biophys Acta* **1809**: 34-45.

Nechaev S, Fargo DC, dos Santos G, Liu L, Gao Y, Adelman K. 2010. Global analysis of short RNAs reveals widespread promoter-proximal stalling and arrest of Pol II in Drosophila. *Science* **327**: 335-338.

Nicodeme E, Jeffrey KL, Schaefer U, Beinke S, Dewell S, Chung C-w, Chandwani R, Marazzi I, Wilson P, Coste H et al. 2010. Suppression of inflammation by a synthetic histone mimic. *Nature* **468**: 1119-1123.

O'Neill LAJ, Golenbock D, Bowie AG. 2013. The history of Toll-like receptors — redefining innate immunity. *Nature Reviews Immunology* **13**: 453-460.

Ogawa S, Lozach J, Benner C, Pascual G, Tangirala RK, Westin S, Hoffmann A, Subramaniam S, David M, Rosenfeld MG et al. 2005. Molecular Determinants of Crosstalk between Nuclear Receptors and Toll-like Receptors. *Cell* **122**: 707-721.

Oh KS, Patel H, Gottschalk RA, Lee WS, Baek S, Fraser IDC, Hager GL, Sung MH. 2017. Anti-Inflammatory Chromatinscape Suggests Alternative Mechanisms of Glucocorticoid Receptor Action. *Immunity* **47**: 298-309 e295.

Ramirez-Carrozzi VR, Braas D, Bhatt DM, Cheng CS, Hong C, Doty KR, Black JC, Hoffmann A, Carey M, Smale ST. 2009. A Unifying Model for the Selective Regulation of Inducible Transcription by CpG Islands and Nucleosome Remodeling. *Cell* **138**: 114-128.

Rao NAS, McCalman MT, Moulos P, Francoijs KJ, Chatziioannou A, Kolisis FN, Alexis MN, Mitsiou DJ, Stunnenberg HG. 2011. Coactivation of GR and NFKB alters the repertoire of their binding sites and target genes. *Genome research* **21**: 1404-1416.

889 Reddy TE, Pauli F, Sprouse RO, Neff NF, Newberry KM, Garabedian MJ, Myers RM. 2009.
890 Genomic determination of the glucocorticoid response reveals unexpected
891 mechanisms of gene regulation. *Genome research* **19**: 2163-2171.
892 Robinson MD, McCarthy DJ, Smyth GK. 2009. edgeR: a Bioconductor package for differential
893 expression analysis of digital gene expression data. *Bioinformatics* **26**: 139-140.
894 Roe JS, Mercan F, Rivera K, Pappin DJ, Vakoc CR. 2015. BET Bromodomain Inhibition
895 Suppresses the Function of Hematopoietic Transcription Factors in Acute Myeloid
896 Leukemia. *Mol Cell* **58**: 1028-1039.
897 Rogatsky I, Adelman K. 2014. Preparing the first responders: building the inflammatory
898 transcriptome from the ground up. *Mol Cell* **54**: 245-254.
899 Sacta MA, Chinenov Y, Rogatsky I. 2016. Glucocorticoid Signaling: An Update from a
900 Genomic Perspective. *Annual Review of Physiology* **78**: 155-180.
901 Schaukowitch K, Joo JY, Liu X, Watts JK, Martinez C, Kim TK. 2014. Enhancer RNA facilitates
902 NELF release from immediate early genes. *Mol Cell* **56**: 29-42.
903 Shang Y, Coppo M, He T, Ning F, Yu L, Kang L, Zhang B, Ju C, Qiao Y, Zhao B et al. 2016. The
904 transcriptional repressor Hes1 attenuates inflammation by regulating transcription
905 elongation. *Nat Immunol* **17**: 930-937.
906 Shi J, Vakoc CR. 2014. The mechanisms behind the therapeutic activity of BET
907 bromodomain inhibition. *Mol Cell* **54**: 728-736.
908 Smale ST, Natoli G. 2014. Transcriptional control of inflammatory responses. *Cold Spring*
909 *Harbor perspectives in biology* **6**: a016261.
910 Smale ST, Tarakhovsky A, Natoli G. 2014. Chromatin contributions to the regulation of
911 innate immunity. *Annual review of immunology* **32**: 489-511.
912 Tong AJ, Liu X, Thomas BJ, Lissner MM, Baker MR, Senagolage MD, Allred AL, Barish GD,
913 Smale ST. 2016. A Stringent Systems Approach Uncovers Gene-Specific Mechanisms
914 Regulating Inflammation. *Cell*.
915 Uhlenhaut NH, Barish Grant D, Yu Ruth T, Downes M, Karunasiri M, Liddle C, Schwalie P,
916 Hübner N, Evans Ronald M. 2013. Insights into Negative Regulation by the
917 Glucocorticoid Receptor from Genome-wide Profiling of Inflammatory Cistromes.
918 *Molecular cell* **49**: 158-171.
919 Weikum ER, de Vera IMS, Nwachukwu JC, Hudson WH, Nettles KW, Kojetin DJ, Ortlund EA.
920 2017a. Tethering not required: the glucocorticoid receptor binds directly to
921 activator protein-1 recognition motifs to repress inflammatory genes. *Nucleic acids*
922 *research* **45**: 8596-8608.
923 Weikum ER, Knuesel MT, Ortlund EA, Yamamoto KR. 2017b. Glucocorticoid receptor
924 control of transcription: precision and plasticity via allostery. *Nature Reviews*
925 *Molecular Cell Biology*.
926 Zhang Y, Liu T, Meyer CA, Eeckhoute J, Johnson DS, Bernstein BE, Nussbaum C, Myers RM,
927 Brown M, Li W et al. 2008. Model-based Analysis of ChIP-Seq (MACS). *Genome*
928 *Biology* **9**: R137.
929 Zhu LJ, Gazin C, Lawson ND, Pagès H, Lin SM, Lapointe DS, Green MR. 2010. ChIPpeakAnno:
930 a Bioconductor package to annotate ChIP-seq and ChIP-chip data. *BMC*
931 *Bioinformatics* **11**: 237.
932
933
934

Figure legends

Figure 1.

GR represses LPS-induced genes via p65-assisted tethering. (**A**) Over 30% of LPS-induced genes (597) in BMDM are repressed by Dex (201; Venn diagram and normalized expression values) and show a pro-inflammatory gene signature (GO analysis). BMDM were untreated (U) or treated with 10 ng/ml LPS +/-100 nM Dex (L and LD) for 1 h, and gene expression levels were determined by RNA-seq (n=2). (**B**) The overlap between ChIP-seq peak calls for GR and p65 in LPS+Dex-treated BMDM (Venn diagram) was determined using *subsetByOverlap* function from GenomicRanges package (Bioconductor) with the minimum overlap of 1 nt (see Methods). *Ab initio* sequence motif discovery and over-representation in each subset of GR or p65 binding peaks was determined using MEME-ChIP (Ma et al. 2014). E-values for the enrichment of the motif are shown. (**C**) Dex- and LPS+Dex-induced GR ChIP-seq peaks are shown (Venn diagram). LPS+Dex-unique peaks are enriched for NF-kB binding sites as indicated by MEME-ChIP analysis as in B. (**D**) Genomic location of p65 and GR binding sites relative to known genomic features is determined by *ChIPpeakAnno* (Bioconductor) (Zhu et al. 2010). (**E**) The distribution of GR binding sites located in a 200 Kb region centered on LPS-induced Dex-repressed genes in BMDM treated with Dex or LPS+Dex (left). Pie-charts show the % of LD-unique GR peaks either genome-wide (center) or those associated with LPS-induced Dex-repressed genes only (right). (**F**) GR and p65 ChIP-seq read density profiles of representative LPS-induced Dex-repressed genes are shown for untreated (U), LPS (L) or LPS+Dex (L+D) treated BMDM.

Also see Fig. 1 – Figure Supplement 1-2 and Supplementary Files 1 and 2.

Figure 2.

Pol 2 and NELF dynamics at different classes of GR-sensitive genes. (**A**) Pol 2 ChIP-seq read density profiles and pausing indexes (PI) for representative paused and non-paused genes

961 in the untreated (U), LPS (L) and LPS+Dex (LD) treated BMDM. (**B**) PI (a ratio of Log-
962 transformed Pol 2 counts at the promoter and gene body in untreated BMDM) was calculated
963 for all LPS-induced Dex-repressed transcript variants with unique 5' ends (see Methods). Genes
964 with PI>1 were considered paused and those with a PI<0.8 non-paused. (**C**) Pol 2 ChIP-seq
965 heat maps of paused (n=62) and non-paused (n=82) transcripts sorted by the PI indexes
966 corresponding to 198 Dex-repressed genes (see Methods) are shown for the U, L and L+D
967 conditions for each individual replica. Only transcripts overlapping Pol 2 peaks in LPS-treated
968 BMDMs as determined by MACS2 are shown. NELF-E heat maps from U BMDM ChIP-seq for
969 the same transcript classes are shown on the right. Heat maps scales are equalized to visualize
970 Pol 2 and NELF distribution across the genes; color scale bars are shown below corresponding
971 maps. (**D**) Average Pol 2 (in each treatment condition) and NELF-E (untreated BMDM)
972 occupancy for each gene class defined in C. The confidence band shows the SEM and 95%
973 confidence interval.
974 Also see Supplementary Files 2 and 3.
975
976 **Figure 3.**
977 **Gene class-specific contribution of NELF to GR-mediated repression.** (**A**) Heat maps show
978 NELF-E occupancy in the U (from Fig. 2C), 1 and 3 h L-treated BMDM for paused and non-
979 paused transcripts. Average occupancy for the paused genes in each condition is graphed as in
980 Fig. 2D. Representative examples of Pol 2 and NELF ChIP-seq read density profiles are shown
981 on the right. (**B**) Pie charts show the percentage of all paused (24%) and non-paused (66%)
982 LPS-induced Dex-repressed genes that exhibit promoter-proximal NELF-E binding in the UNT
983 (86.3 and 31.7%, respectively) and L+D conditions (83.6 and 33.2%, respectively). NELF-E
984 ChIP-seq read density profiles for the L+D condition are shown for a set of representative
985 genes. Red rectangles in *Tnf*, *Myc*, *Errfi1* and *Ccl2* profiles indicate MACS2 NELF-E peaks in
986 the L+D condition. (**C**) NELF-B KO mice were generated as described in Methods. NELF-B

RNA in WT and KO BMDM was quantified by RT-qPCR and normalized to *Actb* (n=5, P<0.0001, two-tailed Student's t-test; error bars are SEM). For western blots, three mice per genotype were used to visualize NELF-B, NELF-E and HSP90 as a loading control (top). Bottom: WT and NELF-B KO BMDM were U or treated with L-/+D for 30 min (*Tnf*) or 1 h (all others) and the expression of indicated genes (matching those in B) was assessed by RT-qPCR, normalized to Actb, and shown as 'fold activation by LPS' over basal levels (=1) and 'fold repression by Dex' (a ratio of L over L+D level of each transcript). *P<0.05, **P<0.01 (Two-tailed Student's t-test). Error bars are SEM. (**D**) The volcano plot comparing gene expression in L+D (1 h) treated BMDM from the WT vs. NELF-B KO mice (n=3) (fold change=1.5, FDR p < 0.05). Pausing indices (PI) of 201 LPS-induced Dex-repressed genes from Fig. 1A are shown in color. (**E**) CDK9 occupancy at selected genes in BMDM treated for 1 h as indicated. n=4-9. **P<0.01, ****P<0.001 (Two-tailed Student's t-test). Error bars are SEM.

Also see Fig. 3 – Figure Supplement 1 and Supplementary File 2.

Figure 4.

GR inhibits H4 acetylation, BRD4 and Mediator assembly at non-paused genes. (**A**) BMDM were treated as indicated, and H4PanAc, H4K5Ac and H4K12Ac at the TSS and indicated kB sites were assessed by ChIP. qPCR signals were normalized to r28S gene and expressed as relative enrichment over normal IgG (=1). A two-tailed Student's t-test was used for comparing means (n≥3; *P<0.05, **P<0.01). Error bars are SEM. (**B**) BMDM were pre-treated with I-BET (10 nM, 100 nM, 1 μM) for 30 min followed by addition of LPS for 30 more min. Gene expression was assessed by RT-qPCR and normalized to that of Actb. A two-tailed Student's t-test was used for comparing means (n≥3; *P<0.05, **P<0.01). Error bars are SEM. (**C**) BRD4 occupancy was assessed by ChIP-qPCR as in A with IgG ChIP as a background metric and expressed as relative enrichment over untreated for each site (=1). A two-tailed Student's t-test was used for comparing means (n≥3, *P<0.05,

P<0.01). (D**) ChIP-seq read density profiles for BRD4, GR and p65 in the U, L or L+D treated BMDM. Purple arrows indicate peaks specifically noted in Results. (**E**) Venn diagrams show overlapping BRD4 peaks for Dex-repressed paused and non-paused genes in the U and L condition. Overlapping peaks were determined as described in Fig. 1 and Methods. (**F**) Med1 and Med12 occupancy is analyzed by ChIP-qPCR as in A (n≥3).

Also see Fig. 4 – Figure Supplement 1 and Supplementary File 2.

Figure 5.

GR-mediated repression of non-paused genes is associated with the diminished p300 function. (**A**) p300 occupancy at indicated kB binding sites is evaluated as in Fig. 4C (n≥3). (**B**) p300 occupancy at indicated kB binding sites is evaluated as in A (n≥3; top panel). p65 ChIP-seq read density distribution in U-, L- or L+D treated BMDM for corresponding kB binding sites is shown (bottom panel). Expression level (log(CPM) values) for LPS-induced Dex-insensitive genes as determined by RNA-seq in Fig. 1A for the WT BMDM (untreated, LPS 1 h, L+D 1 h, n=2, right panel). (**C**) BMDM were treated with LPS for 30 min followed by addition of 5 μM or 10 μM C646 for another 1 h. The expression of indicated genes was assessed as described in Fig. 4B (n≥3). (**D**) RAW264.7 cells were transfected with increasing amounts of pcDNA3-p300 or pcDNA3-p300(ΔHAT) (0, 50, 100 and 150 ng/well) as described in Methods. Cells were treated with 100 ng/ml LPS +/- 100 nM Dex for 1 h. Gene expression was analyzed as described in Fig. 3C (n≥3).

LEGENDS TO SUPPLEMENTARY FIGURES

Figure 1 – Figure Supplement 1. Characterization of GR cistromes in Dex- and LPS+Dex-treated BMDM. (**A**) Venn diagram comparison of GR peak sets from ChIP-seq replicates in BMDM treated as indicated (left) and between treatments (right). The union of peak sets was constructed for each condition. Read counts were determined for each peak in condition-specific peak union sets for each replicate; a plot of log transformed per peak read counts for GR replicas is shown for each treatment condition; r_s - Spearman's correlation between replicas (left, bottom). (**B**) The centrality enrichment analysis of binding motifs identified by *ab initio* prediction with MEME was performed using CentriMo program of MEME suite. Significant distribution profiles relative to the peak midpoint are shown for several subsets of peaks identified by GR and p65 ChIP-seq. Left: GR-unique peaks from GR:p65 cistromes in LPS+Dex-treated BMDM (Fig. 1B). Middle: GR, L+D peaks overlapping p65, L+D peaks. Right: GR, D peaks overlapping GR, L+D peaks (Fig. 1C). (**C**) Distribution of gene and intron length in Dex-repressed genes compared to all expressed genes in mouse BMDM. (**D**) Cross-correlation plots for GR ChIP-seq datasets generated in this study. Relative strand cross-correlations were calculated using CLC BIO Genomics Workbench.

Figure 1 – Figure Supplement 2. Characterization of p65 cistromes in LPS- and LPS+Dex-treated BMDM. (**A**) Venn diagram comparison of p65 peak sets from ChIP-seq replicates in BMDM treated as indicated (left) and between treatments (right). The union of peak sets was constructed for each condition. Read counts were determined for each peak in condition-specific peak union sets; a plot of log transformed per peak read counts for p65 replicas is shown for each treatment condition; r_s - Spearman's correlation between replicas (left, bottom). (**B**) p65 peaks distribution in LPS- and LPS+Dex-treated BMDM near Dex-repressed genes from Fig. 1A (+/- 100 Kb) (**C**) Cross-correlation plots for p65 ChIP-seq datasets generated in this study. Relative strand cross-correlations were calculated using CLC BIO Genomics Workbench.

Figure 3 - Figure Supplement 1. Characterization of Pol 2 and NELF cistromes in BMDM. (**A**) Cross-correlation plots for Pol 2 and NELF-E ChIP-seq datasets generated in this study. Relative strand cross-correlations were calculated using CLC BIO Genomics Workbench. A plot of log transformed per gene read counts for Pol 2 replicas is shown for each treatment condition; r_s - Spearman's correlation between replicas. (**B**) A pie chart shows the percentage of all paused (23%) and non-paused (70%) LPS-induced Dex-insensitive transcripts that exhibit NELF-E binding (81.1 and 44.2 %, respectively) in untreated BMDM. Paused and non-paused transcripts were identified as described in Methods. (**C**) RNA-seq expression levels of indicated genes in

untreated WT and NELF-B KO BMDM (n=2). (**D**) The volcano plots compare gene expression in L+D (1 h) treated WT vs. NELF-B KO BMDM (n=3, fold change=1.5, FDR $p < 0.05$). Pausing indexes for LPS-induced Dex-insensitive genes from Fig. 1A (left) and LPS-insensitive genes (right) are shown in colors, as indicated.

Figure 4 - Figure Supplement 1. Characterization of BRD4 cistromes in BMDM. (**A**) Venn diagram comparisons of BRD4 peak numbers in LPS-treated vs. untreated BMDM in indicated groups of genes. The intersection of individual replica peak sets was constructed for each condition. (**B**) The average occupancy of BRD4 in each treatment condition at the LPS-induced Dex-repressed genes' (left) promoters and (right) L-derived BRD4:p65 overlapping peaks. The occupancy profiles showing the mean score were calculated using *genomation* package. The band surrounding the mean score distribution shows SEM and 95 % confidence interval for the mean. (**C**) Cross-correlation plots for BRD4 ChIP-seq datasets generated in this study. Relative strand cross-correlations were calculated using CLC BIO Genomics Workbench. Read counts were determined for each peak in condition-specific peak union sets; a plot of log transformed per peak read counts for Brd4 replicas is shown for each treatment condition; r_s - Spearman's correlation between replicas.

Figure 1

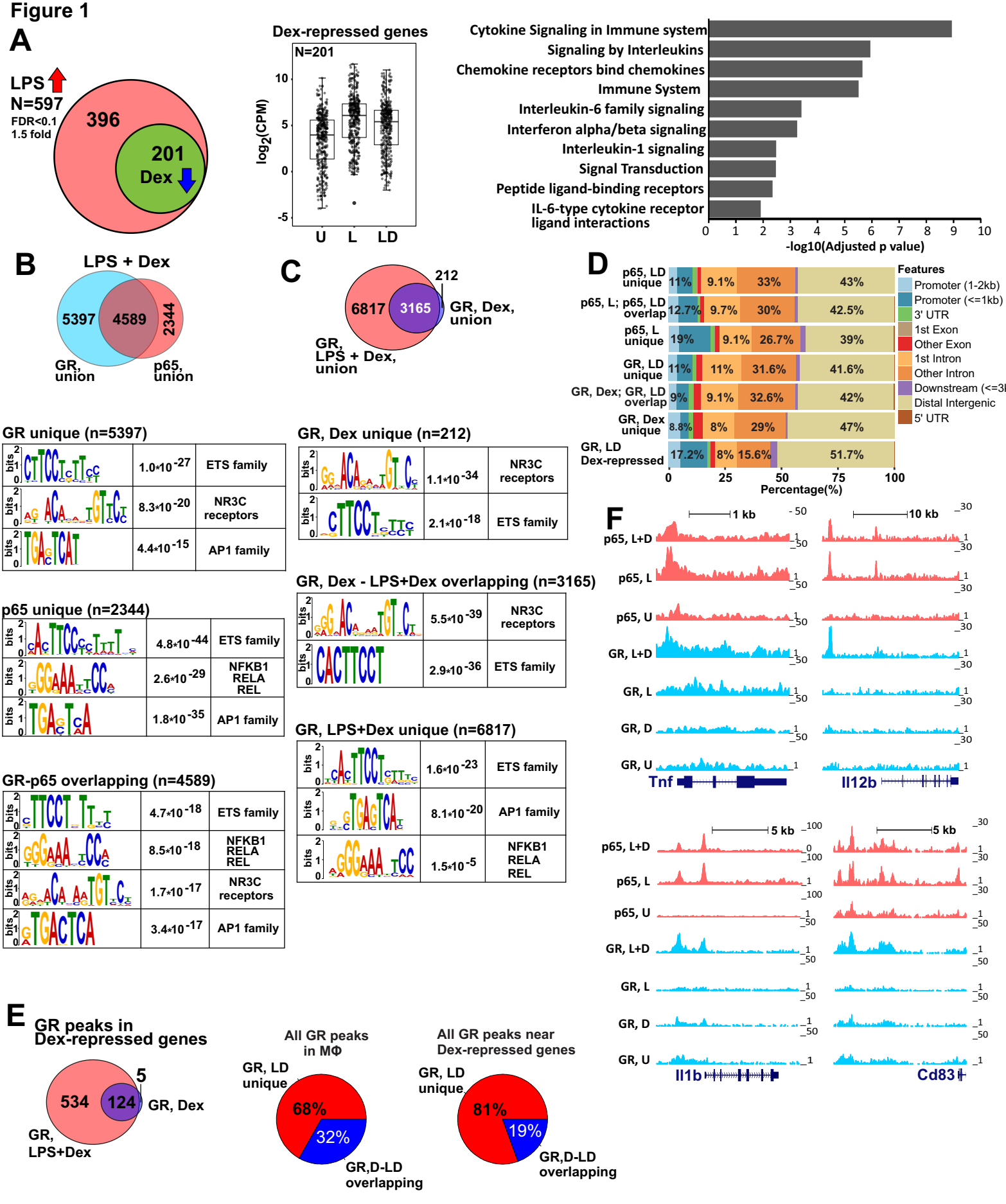
A
LPS
N=597
FDR<0.1
1.5 fold
396
201
Dex
Dex-repressed genes
N=201
log2(CPM)
U
L
LD
Cytokine Signaling in Immune system
Signaling by Interleukins
Chemokine receptors bind chemokines
Immune System
Interleukin-6 family signaling
Interferon alpha/beta signaling
Interleukin-1 signaling
Signal Transduction
Peptide ligand-binding receptors
IL-6-type cytokine receptor ligand interactions
-log10(Adjusted p value)
B
LPS + Dex
5397
4589
2344
GR, union
p65, union
C
6817
3165
212
GR, Dex, union
GR, LPS + Dex, union
D
p65, LD unique
p65, L; p65, LD overlap
p65, L unique
GR, LD unique
GR, Dex; GR, LD overlap
GR, Dex unique
GR, LD Dex-repressed
Features
Promoter (1-2kb)
Promoter (<=1kb)
3' UTR
1st Exon
Other Exon
1st Intron
Other Intron
Downstream (<=3kb)
Distal Intergenic
5' UTR
Percentage(%)
GR unique (n=5397)
1.0*10-27
ETS family
8.3*10-20
NR3C receptors
4.4*10-15
AP1 family
GR, Dex unique (n=212)
1.1*10-34
NR3C receptors
2.1*10-18
ETS family
p65 unique (n=2344)
4.8*10-44
ETS family
2.6*10-29
NFKB1 RELA REL
1.8*10-35
AP1 family
GR, Dex - LPS+Dex overlapping (n=3165)
5.5*10-39
NR3C receptors
2.9*10-36
ETS family
GR-p65 overlapping (n=4589)
4.7*10-18
ETS family
8.5*10-18
NFKB1 RELA REL
1.7*10-17
NR3C receptors
3.4*10-17
AP1 family
GR, LPS+Dex unique (n=6817)
1.6*10-23
ETS family
8.1*10-20
AP1 family
1.5*10-5
NFKB1 RELA REL
F
1 kb
10 kb
p65, L+D
p65, L
p65, U
GR, L+D
GR, L
GR, D
GR, U
Tnf
Il12b
5 kb
Il1b
Cd83
E
GR peaks in Dex-repressed genes
534
124
5
GR, Dex
GR, LPS+Dex
All GR peaks in MΦ
GR, LD unique
68%
32%
GR,D-LD overlapping
All GR peaks near Dex-repressed genes
GR, LD unique
81%
19%
GR,D-LD overlapping

Figure 2

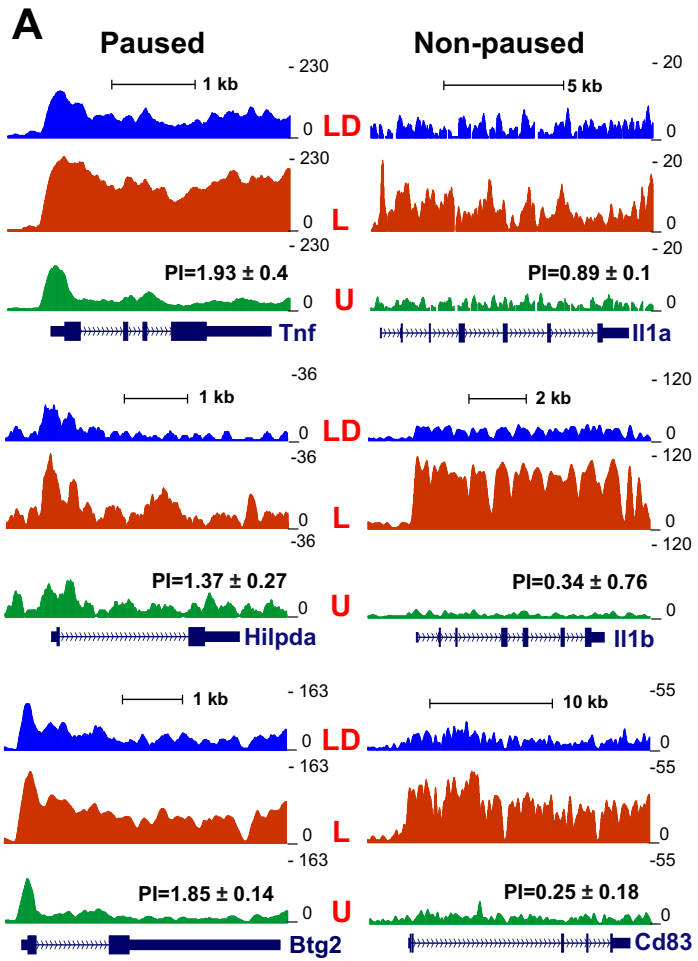
A
Paused
Non-paused
1 kb
5 kb
LD
L
U
PI=1.93 ± 0.4
PI=0.89 ± 0.1
Tnf
Il1a
2 kb
PI=1.37 ± 0.27
PI=0.34 ± 0.76
Hilpda
Il1b
10 kb
PI=1.85 ± 0.14
PI=0.25 ± 0.18
Btg2
Cd83

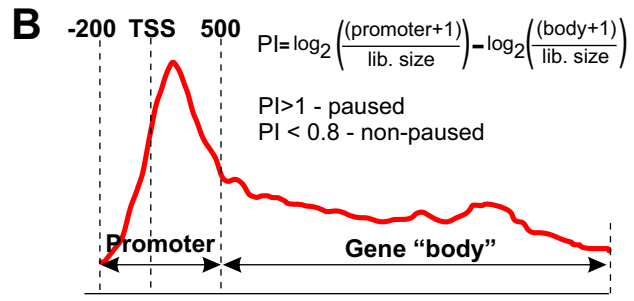
B
-200 TSS 500
PI= log2((promoter+1)/lib. size) − log2((body+1)/lib. size)
PI>1 - paused
PI < 0.8 - non-paused
Promoter
Gene "body"

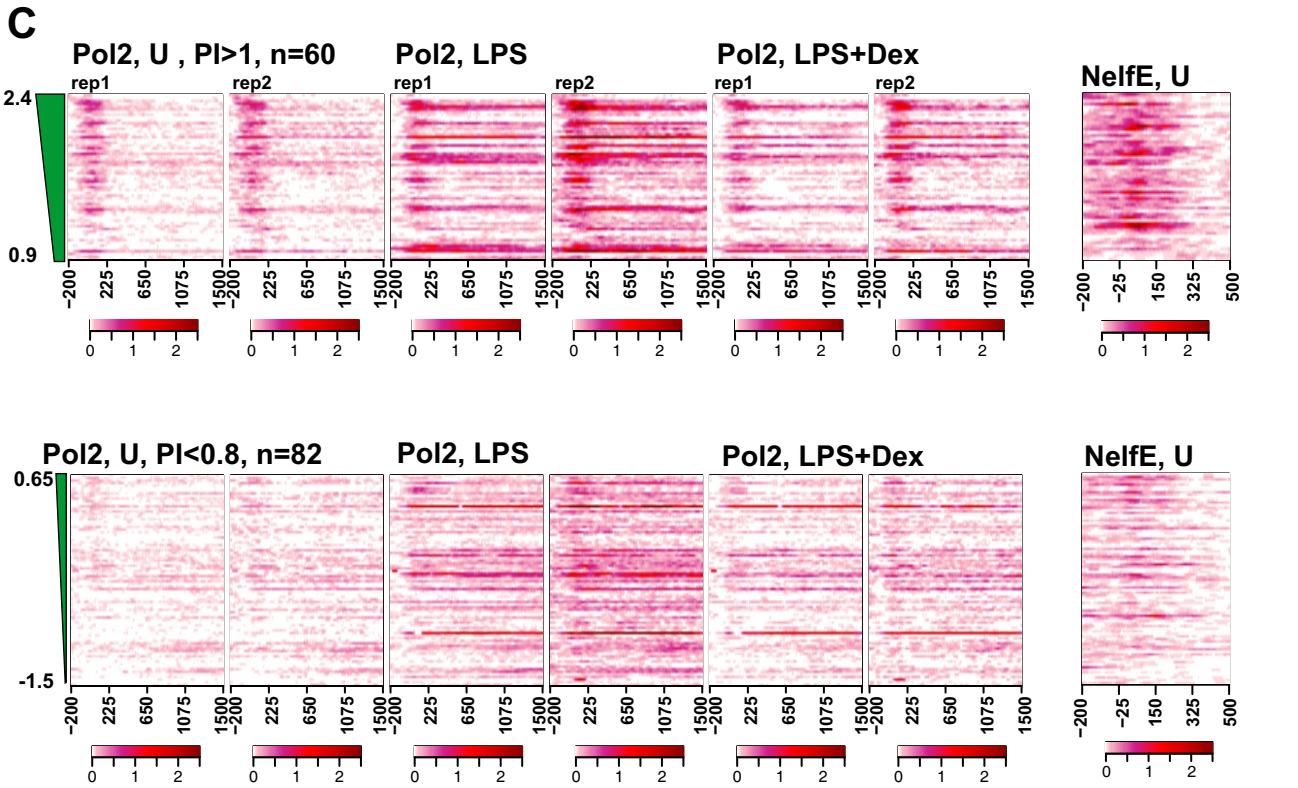
C
Pol2, U , PI>1, n=60
Pol2, LPS
Pol2, LPS+Dex
NelfE, U
rep1
rep2
Pol2, U, PI<0.8, n=82

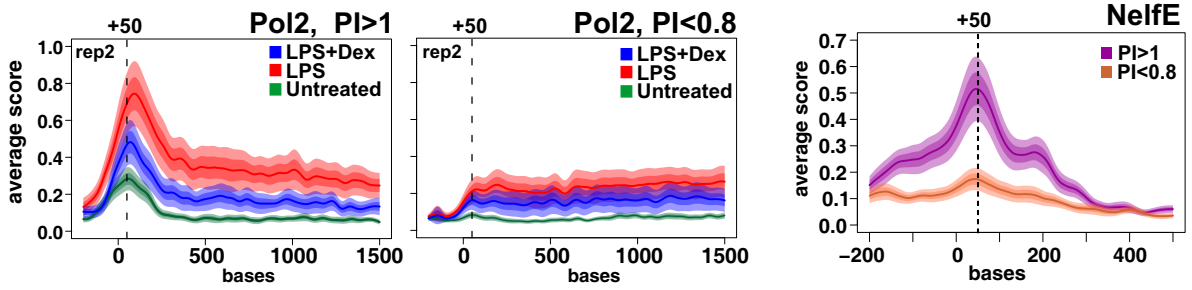
D
Pol2, PI>1
Pol2, PI<0.8
NelfE
LPS+Dex
LPS
Untreated
PI>1
PI<0.8
average score
bases

Figure 3

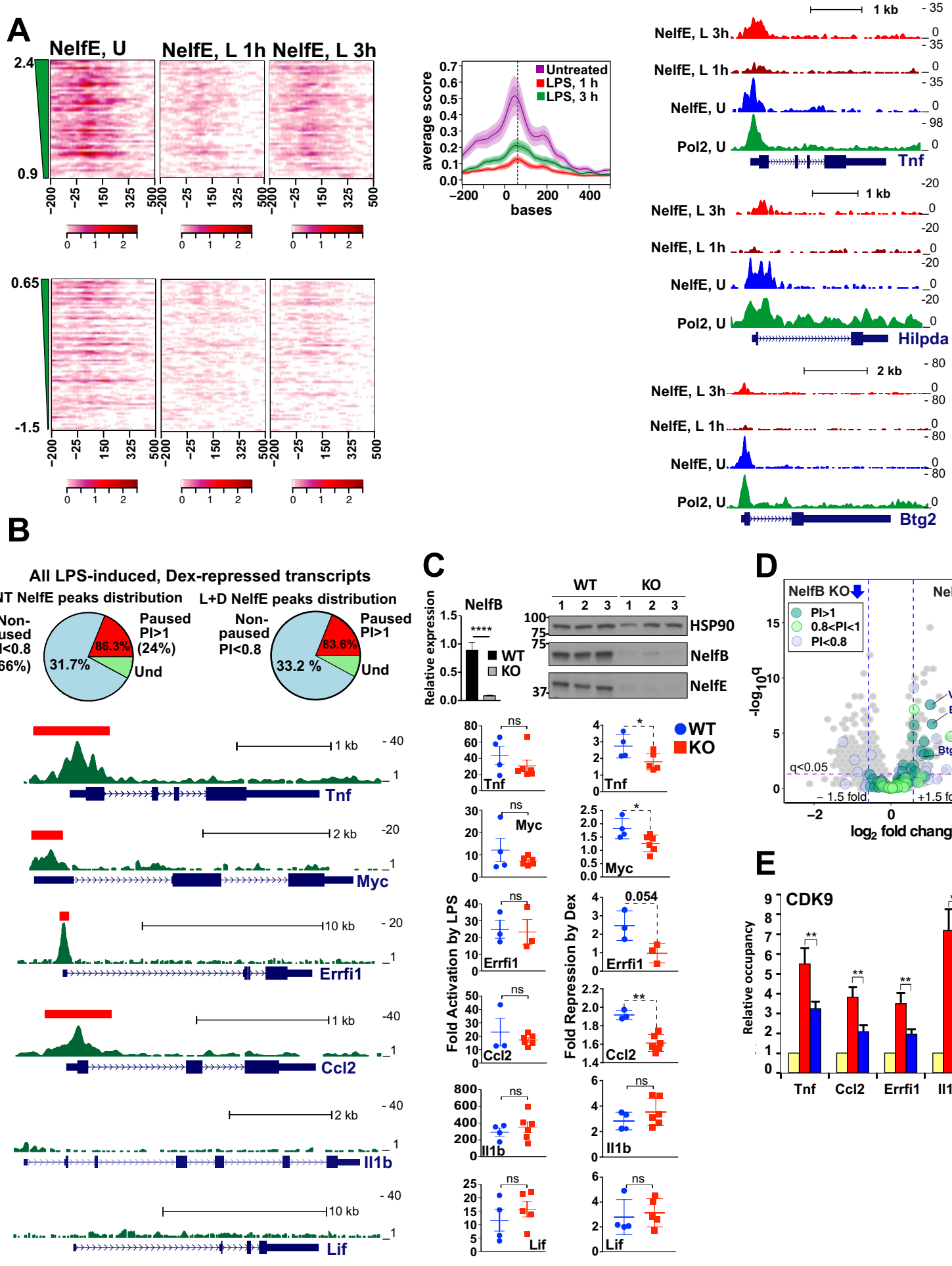
A
NelfE, U
NelfE, L 1h
NelfE, L 3h
2.4
0.9
0.65
-1.5
average score
Untreated
LPS, 1 h
LPS, 3 h
bases
1 kb
2 kb
Tnf
Hilpda
Btg2
B
All LPS-induced, Dex-repressed transcripts
UNT NelfE peaks distribution
L+D NelfE peaks distribution
Non-paused PI<0.8 (66%)
Paused PI>1 (24%)
Und
31.7%
86.3%
Non-paused PI<0.8
Paused PI>1
Und
33.2 %
83.6%
10 kb
Myc
Errfi1
Ccl2
Il1b
Lif
C
NelfB
Relative expression
WT
KO
HSP90
NelfB
NelfE
Fold Activation by LPS
Fold Repression by Dex
ns
0.054
D
NelfB KO
NelfB KO
PI>1
0.8<PI<1
PI<0.8
Phda1
Vegfa
Errfi1
Hspa1a
Btg2
Hspa1b
q<0.05
– 1.5 fold
+1.5 fold
log2 fold change
E
CDK9
Relative occupancy
U
L
LD
Tnf
Ccl2
Errfi1
Il1b
Lif

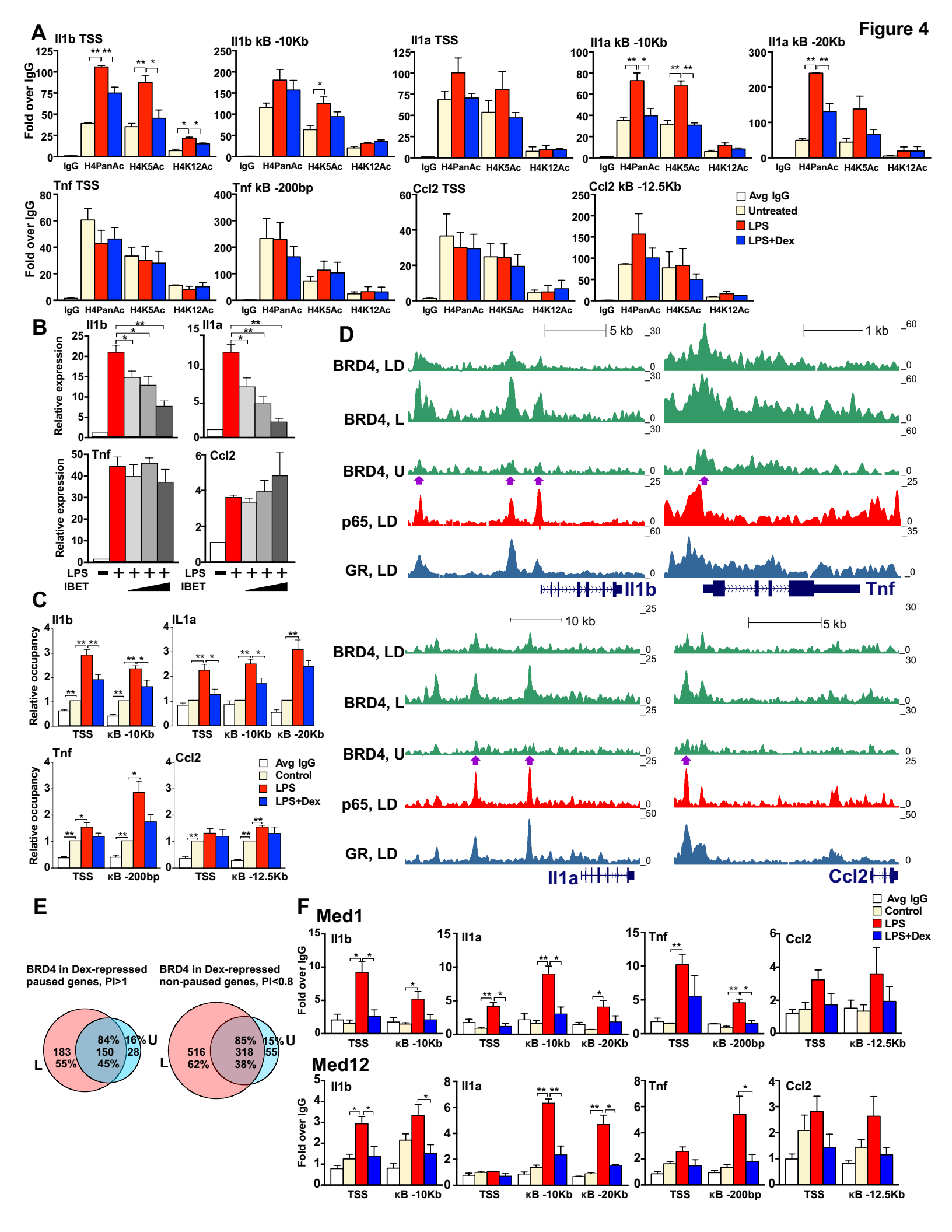
Figure 4
A
Il1b TSS
Il1b kB -10Kb
Il1a TSS
Il1a kB -10Kb
Il1a kB -20Kb
Tnf TSS
Tnf kB -200bp
Ccl2 TSS
Ccl2 kB -12.5Kb
Fold over IgG
IgG H4PanAc H4K5Ac H4K12Ac
Avg IgG
Untreated
LPS
LPS+Dex
B
Il1b
Il1a
Tnf
Ccl2
Relative expression
LPS
IBET
C
Il1b
IL1a
Tnf
Ccl2
Relative occupancy
TSS
κB -10Kb
κB -20Kb
κB -200bp
κB -12.5Kb
Avg IgG
Control
LPS
LPS+Dex
D
BRD4, LD
BRD4, L
BRD4, U
p65, LD
GR, LD
5 kb
1 kb
10 kb
Il1b
Tnf
Il1a
Ccl2
E
BRD4 in Dex-repressed paused genes, PI>1
BRD4 in Dex-repressed non-paused genes, PI<0.8
L
U
183 55%
84% 150 45%
16% 28
516 62%
85% 318 38%
15% 55
F
Med1
Med12
Il1b
Il1a
Tnf
Ccl2
Fold over IgG
TSS
κB -10Kb
κB -20Kb
κB -200bp
κB -12.5Kb
Avg IgG
Control
LPS
LPS+Dex

Figure 5

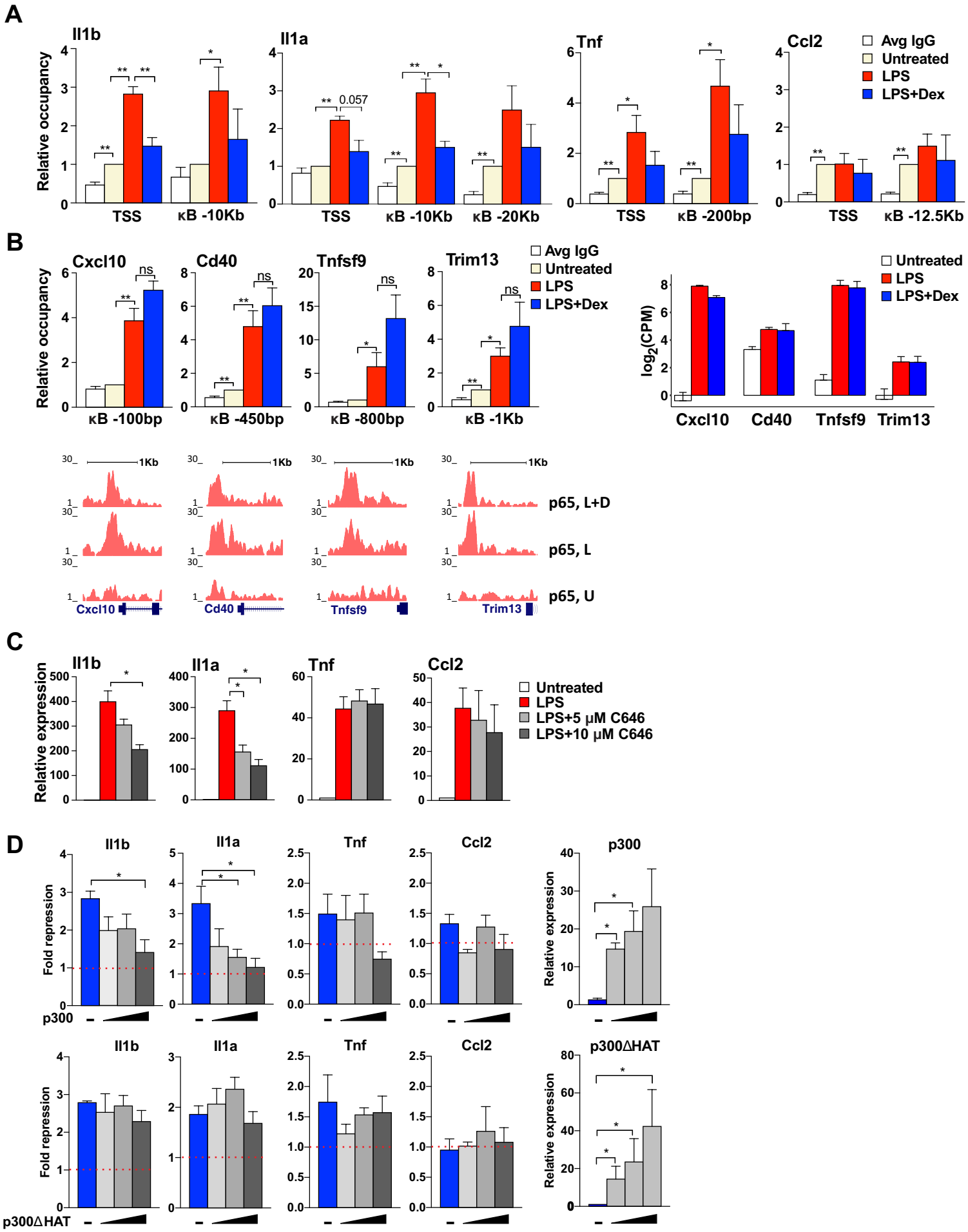
A
Il1b
Il1a
Tnf
Ccl2
Relative occupancy
Avg IgG
Untreated
LPS
LPS+Dex
TSS
κB -10Kb
κB -20Kb
κB -200bp
κB -12.5Kb
0.057
B
Cxcl10
Cd40
Tnfsf9
Trim13
ns
κB -100bp
κB -450bp
κB -800bp
κB -1Kb
log2(CPM)
1Kb
p65, L+D
p65, L
p65, U
C
Relative expression
LPS+5 μM C646
LPS+10 μM C646
D
p300
Fold repression
p300ΔHAT

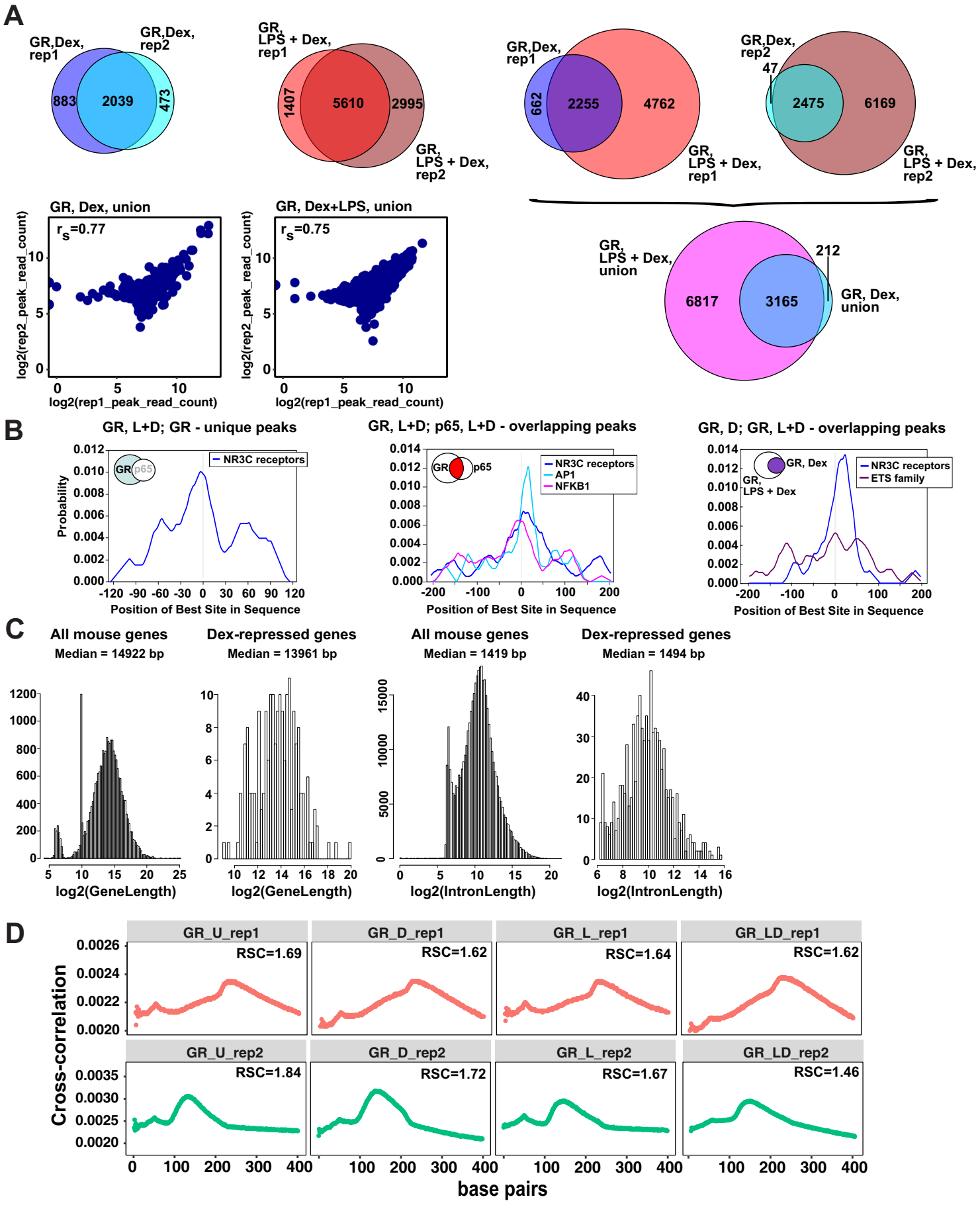
A
GR,Dex, rep1
GR,Dex, rep2
883
2039
473
GR, LPS + Dex, rep1
GR, LPS + Dex, rep2
1407
5610
2995
GR,Dex, rep1
GR, LPS + Dex, rep1
662
2255
4762
GR,Dex, rep2
GR, LPS + Dex, rep2
47
2475
6169
GR, Dex, union
r_s=0.77
log2(rep2_peak_read_count)
log2(rep1_peak_read_count)
GR, Dex+LPS, union
r_s=0.75
GR, LPS + Dex, union
GR, Dex, union
6817
3165
212
B
GR, L+D; GR - unique peaks
NR3C receptors
Probability
Position of Best Site in Sequence
GR, L+D; p65, L+D - overlapping peaks
NR3C receptors
AP1
NFKB1
GR, D; GR, L+D - overlapping peaks
GR, Dex
GR, LPS + Dex
NR3C receptors
ETS family
C
All mouse genes
Median = 14922 bp
Dex-repressed genes
Median = 13961 bp
All mouse genes
Median = 1419 bp
Dex-repressed genes
Median = 1494 bp
log2(GeneLength)
log2(IntronLength)
D
GR_U_rep1
GR_D_rep1
GR_L_rep1
GR_LD_rep1
GR_U_rep2
GR_D_rep2
GR_L_rep2
GR_LD_rep2
RSC=1.69
RSC=1.62
RSC=1.64
RSC=1.62
RSC=1.84
RSC=1.72
RSC=1.67
RSC=1.46
Cross-correlation
base pairs

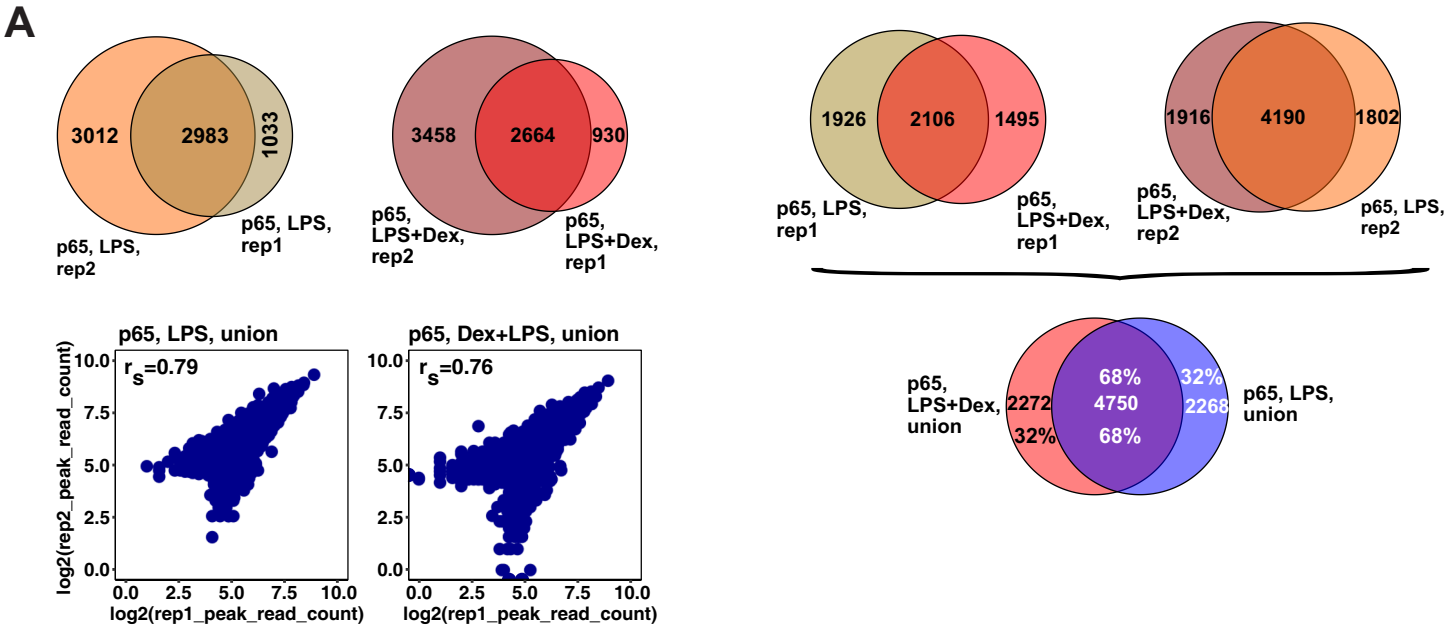
A
3012
2983
1033
p65, LPS, rep2
p65, LPS, rep1
3458
2664
930
p65, LPS+Dex, rep2
p65, LPS+Dex, rep1
1926
2106
1495
p65, LPS, rep1
p65, LPS+Dex, rep1
1916
4190
1802
p65, LPS+Dex, rep2
p65, LPS, rep2
p65, LPS, union
p65, Dex+LPS, union
r_s=0.79
r_s=0.76
log2(rep2_peak_read_count)
log2(rep1_peak_read_count)
log2(rep1_peak_read_count)
p65, LPS+Dex, union
2272
32%
68%
4750
68%
32%
2268
p65, LPS, union

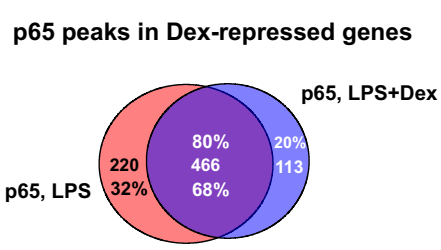
B
p65 peaks in Dex-repressed genes
p65, LPS+Dex
p65, LPS
220
32%
80%
466
68%
20%
113

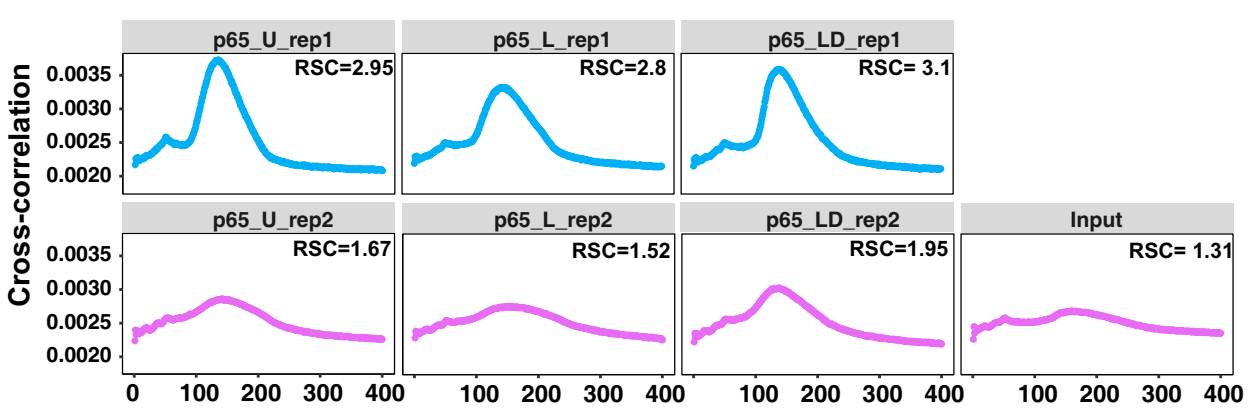
C
p65_U_rep1
p65_L_rep1
p65_LD_rep1
p65_U_rep2
p65_L_rep2
p65_LD_rep2
Input
RSC=2.95
RSC=2.8
RSC= 3.1
RSC=1.67
RSC=1.52
RSC=1.95
RSC= 1.31
Cross-correlation

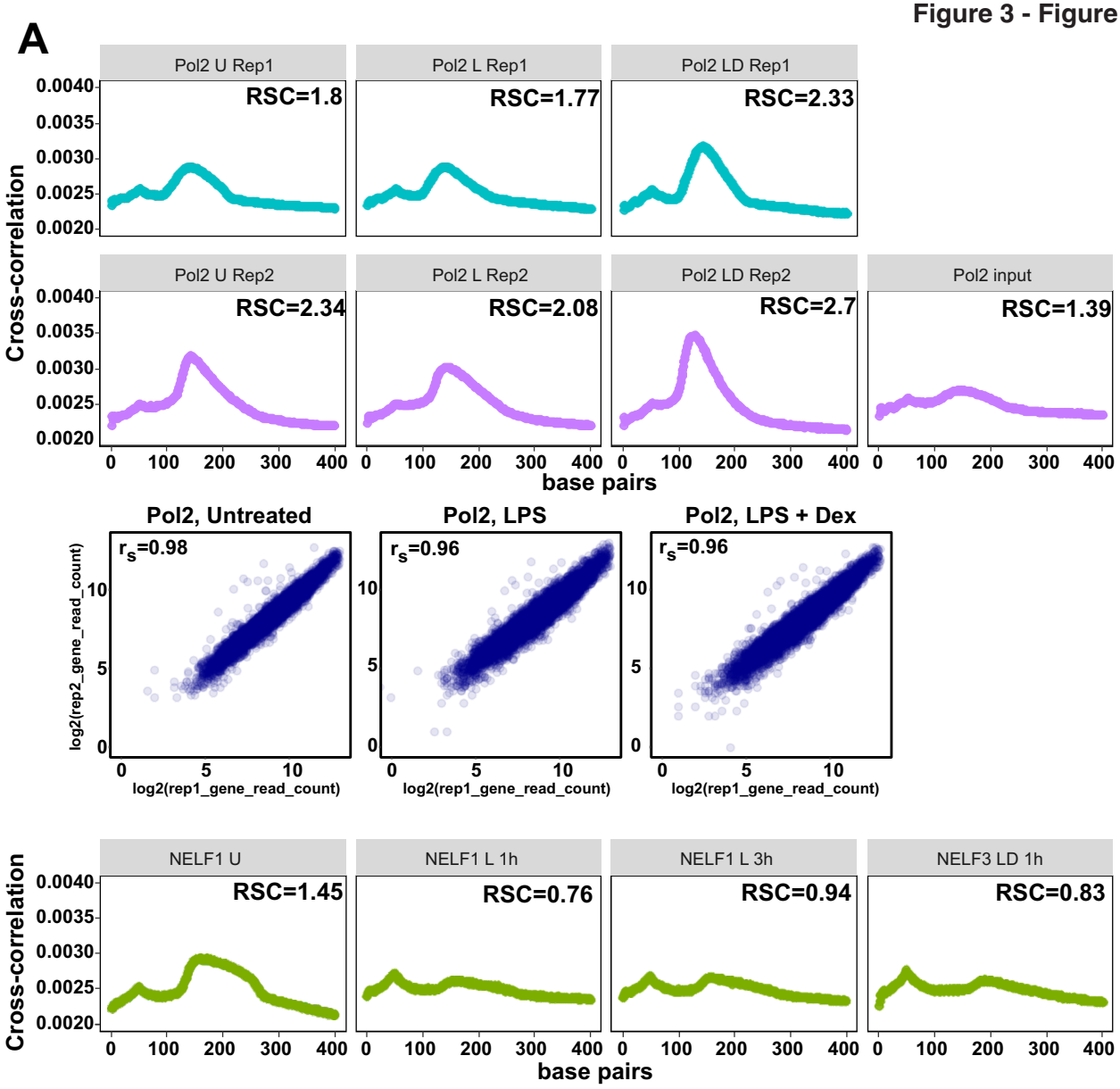
A
Pol2 U Rep1
RSC=1.8
Pol2 L Rep1
RSC=1.77
Pol2 LD Rep1
RSC=2.33
Pol2 U Rep2
RSC=2.34
Pol2 L Rep2
RSC=2.08
Pol2 LD Rep2
RSC=2.7
Pol2 input
RSC=1.39
Cross-correlation
base pairs
Pol2, Untreated
Pol2, LPS
Pol2, LPS + Dex
rs=0.98
rs=0.96
rs=0.96
log2(rep2_gene_read_count)
log2(rep1_gene_read_count)
NELF1 U
RSC=1.45
NELF1 L 1h
RSC=0.76
NELF1 L 3h
RSC=0.94
NELF3 LD 1h
RSC=0.83
B
All LPS-induced, Dex-insensitive transcripts
UNT NelfE peaks distribution
Paused, PI>1
23%
Non-paused,
PI<0.8
70%
81.1 %
44.2 %
Undefined
C
WT
NelfB KO
log2(CPM)
Tnf
Myc
Errfi1
Ccl2
Il1b
Lif
D
LPS-induced Dex-insensitive genes
LPS-insensitive genes
NelfB KO
NelfB KO
PI>1
0.8<PI<1
PI<0.8
-log10q
q<0.05
– 1.5 fold
+1.5 fold
log2 fold change

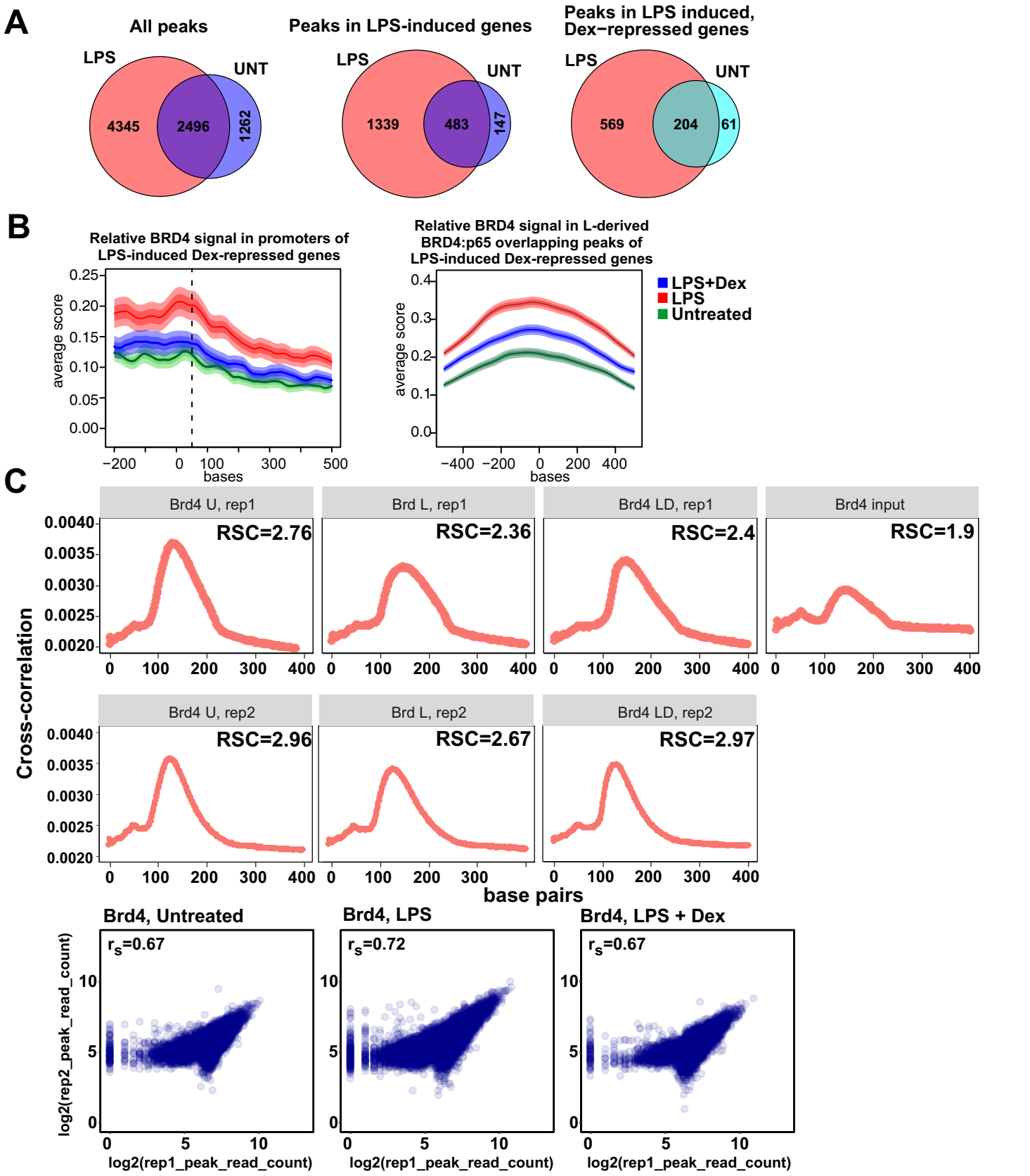
A
All peaks
LPS
UNT
4345
2496
1262
Peaks in LPS-induced genes
LPS
UNT
1339
483
147
Peaks in LPS induced, Dex−repressed genes
LPS
UNT
569
204
61
B
Relative BRD4 signal in promoters of LPS-induced Dex-repressed genes
average score
bases
Relative BRD4 signal in L-derived BRD4:p65 overlapping peaks of LPS-induced Dex-repressed genes
average score
bases
LPS+Dex
LPS
Untreated
C
Cross-correlation
Brd4 U, rep1
RSC=2.76
Brd L, rep1
RSC=2.36
Brd4 LD, rep1
RSC=2.4
Brd4 input
RSC=1.9
Brd4 U, rep2
RSC=2.96
Brd L, rep2
RSC=2.67
Brd4 LD, rep2
RSC=2.97
base pairs
Brd4, Untreated
rs=0.67
Brd4, LPS
rs=0.72
Brd4, LPS + Dex
rs=0.67
log2(rep2_peak_read_count)
log2(rep1_peak_read_count)